Inorg. Chem. **2003**, *42*, 7472–7488

First Row Divalent Transition Metal Complexes of Aryl-Appended Tris((pyridyl)methyl)amine Ligands: Syntheses, Structures, Electrochemistry, and Hydroxamate Binding Properties

Magdalena M. Makowska-Grzyska,[†] Ewa Szajna,[†] Crystal Shipley,[†] Atta M. Arif,[‡] Michael H. Mitchell,[§] Jason A. Halfen,[§] and Lisa M. Berreau*,[†]

Department of Chemistry and Biochemistry, Utah State University, Logan, Utah 84322-0300, Department of Chemistry, University of Utah, Salt Lake City, Utah 84112, and Department of Chemistry, University of Wisconsin—Eau Claire, Eau Claire, Wisconsin 54702

Received July 12, 2003

Divalent manganese, cobalt, nickel, and zinc complexes of 6-Ph_2TPA (*N*,*N*-bis((6-phenyl-2-pyridyl)methyl)-*N*-((2-pyridyl)methyl)amine; $[(6\text{-}Ph_2TPA)Mn(CH_3OH)_3](ClO_4)_2$ (**1**), $[(6\text{-}Ph_2TPA)Co(CH_3CN)](ClO_4)_2$ (**2**), $[(6\text{-}Ph_2TPA)Ni(CH_3CN)(CH_3OH)](ClO_4)_2$ (**3**), $[(6\text{-}Ph_2TPA)Zn(CH_3CN)](ClO_4)_2$ (**4**)) and 6-$(Me_2Ph)_2$TPA (*N*,*N*-bis((6-(3,5-dimethyl)phenyl-2-pyridyl)methyl)-*N*-((2-pyridyl)methyl)amine; $[(6\text{-}(Me_2Ph)_2TPA)Ni(CH_3CN)_2](ClO_4)_2$ (**5**) and $[(6\text{-}(Me_2Ph)_2TPA)Zn(CH_3CN)](ClO_4)_2$ (**6**)) have been prepared and characterized. X-ray crystallographic characterization of **1A·CH_3OH** and **1B·2CH_3OH** (differing solvates of **1**), **2·2CH_3CN**, **3·CH_3OH**, **4·2CH_3CN**, and **6·2.5CH_3CN** revealed mononuclear cations with one to three coordinated solvent molecules. In **1A·CH_3OH** and **1B·2CH_3OH**, one phenyl-substituted pyridyl arm is not coordinated and forms a secondary hydrogen-bonding interaction with a manganese bound methanol molecule. In **2·2CH_3CN**, **3·CH_3OH**, **4·2CH_3CN**, and **6·2.5CH_3CN**, all pyridyl donors of the 6-Ph_2TPA and 6-$(Me_2Ph)_2$TPA ligands are coordinated to the divalent metal center. In the cobalt, nickel, and zinc derivatives, CH/π interactions are found between a bound acetonitrile molecule and the aryl appendages of the 6-Ph_2TPA and 6-$(Me_2Ph)_2$TPA ligands. ^{1}H NMR spectra of **4** and **6** in CD_3NO_2 solution indicate the presence of CH/π interactions, as an upfield-shifted methyl resonance for a bound acetonitrile molecule is present. Examination of the cyclic voltammetry of **1**–**3** and **5** revealed no oxidative (M(II)/M(III)) couples. Admixture of equimolar amounts of 6-Ph_2TPA, $M(ClO_4)_2\cdot 6H_2O$, and $Me_4NOH\cdot 5H_2O$, followed by the addition of an equimolar amount of acetohydroxamic acid, yielded the acetohydroxamate complexes $[((6\text{-}Ph_2TPA)Mn)_2(\mu\text{-}ONHC(O)CH_3)_2](ClO_4)_2$ (**8**), $[(6\text{-}Ph_2TPA)Co(ONHC(O)CH_3)](ClO_4)_2$ (**9**), $[(6\text{-}Ph_2TPA)Ni(ONHC(O)CH_3)](ClO_4)_2$ (**10**), and $[(6\text{-}Ph_2TPA)Zn(ONHC(O)CH_3)](ClO_4)_2$ (**11**), all of which were characterized by X-ray crystallography. The Mn(II) complex **8·0.75CH_3CN·0.75Et_2O** exhibits a dinuclear structure with bridging hydroxamate ligands, whereas the Co(II), Ni(II), and Zn(II) derivatives all exhibit mononuclear six-coordinate structures with a chelating hydroxamate ligand.

Introduction

The chemical reactivity of catalytically active metal centers in metalloenzymes is influenced by many factors, including the number and orientation of coordination sites occupied by labile ligands (e.g., water) that may be displaced by substrate or inhibitor binding, and the secondary environment surrounding the metal center. Interesting biological metal sites for which no model systems have been reported to date include the histidine-rich mononuclear Mn(II) centers in oxalate oxidase[1] and oxalate decarboxylase,[2,3] and the mononuclear Ni(II) center in acireductone dioxygenase.[4] These enzymes have in common (1) a six-coordinate divalent metal center situated in a largely hydrophobic active site and having two water occupied coordination sites, and (2) proposed mechanistic pathways that involve the oxidation of a substrate or intermediate that may be coordinated to

* To whom correspondence should be addressed. E-mail: berreau@cc.usu.edu. Phone: (435) 797-1625. Fax: (435) 797-3390.
† Utah State University.
‡ University of Utah.
§ University of Wisconsin—Eau Claire.

(1) (a) Woo, E.-J.; Dunwell, J. M.; Goodenough, P. W.; Marvier, A. C.; Pickersgill, R. W. *Nat. Struct. Biol.* **2000**, *11*, 1036−1040. (b) Woo, E.-J.; Dunwell, J. M.; Goodenough, P. W.; Pickersgill, R. W. *FEBS Lett.* **1998**, *437*, 87−90.
(2) Anand, R.; Dorrestein, P. C.; Kinsland, C.; Begley, T. P.; Ealick, S. E. *Biochemistry* **2002**, *41*, 7659−7669.

10.1021/ic034810y CCC: $25.00
Published on Web 10/15/2003

the metal center via two oxygen donors to form a five-membered chelate ring.[3a,4b] Notably, five-membered chelate rings involving a coordinated substrate are also proposed to form during isomerization reactions mediated by the mononuclear active site metal centers in glyoxalase I (human, Zn^{2+}; *E. coli*, Ni^{2+}; isomerization of a hemithioacetal substrate).[5]

In the work described herein, we have evaluated the feasibility of using aryl-substituted tris((pyridyl)methyl)amine ligand derivatives to form mononuclear metal complexes that exhibit several key features. These include the following: (1) a hydrophobic environment surrounding a divalent metal center having one or more solvent-occupied coordination sites, (2) stability of the divalent metal oxidation state with respect to oxidation, and (3) an ability to maintain a mononuclear structure in derivative complexes having a coordinated chelating anion. While aryl-substituted tris((pyridyl)methyl)amine (TPA) ligands have received recent attention in the literature for many applications, including as building blocks for copper-containing molecular recognition systems,[6] hemilabile ligands for Fe(II/III) derivatives,[7] and ligand systems wherein an internal aromatic substrate is present for Fe(II)/ROOH reactivity studies,[8] to our knowledge such ligands have received minimal attention in regard to their utility for developing chemistry relevant to several other mononuclear divalent metal sites in metalloenzymes.[9] Herein we report the synthesis and comprehensive characterization of two families of complexes supported by aryl-appended TPA ligands.

Experimental Section

General Methods. All reagents and solvents were obtained from commercial sources and were used as received unless otherwise noted. Solvents were dried according to published procedures and were distilled under N_2 prior to use.[10] Air-sensitive reactions were performed in a MBraun Unilab glovebox under an atmosphere of purified N_2.

Physical Methods. UV−vis spectra were recorded on a Hewlett-Packard 8453 diode array spectrophotometer. IR spectra were recorded on a Shimadzu FTIR-8400 spectrometer as KBr pellets, neat films between NaCl plates, or solution spectra in CH_3CN (∼100 mM). Low resolution electron impact mass spectra (LRE-IMS) were obtained on a Shimadzu QP500 GC/MS equipped with a 30 m HP-5 (cross-linked 5% PhMe-silicone) column. ^1H and $^{13}C\{^1H\}$ NMR spectra were recorded on a JEOL GSX-270 or Bruker ARX-400 spectrometer. Chemical shifts (in ppm) are referenced to the residual solvent peak(s) in CD_3CN (^1H, 1.94 (quintet); $^{13}C\{^1H\}$, 1.39 (heptet) ppm), CD_3OD (^1H, 3.31 (pentet); $^{13}C\{^1H\}$, 49.15 (heptet) ppm), and $CDCl_3$ (^1H, 7.25 (singlet);$^{13}C\{^1H\}$, 77.23 (triplet) ppm). Room-temperature magnetic susceptibilities were determined by the Evans method.[11] Electrochemical experiments were conducted with a BAS CV50 potentiostat, using a platinum disk working electrode, a silver wire pseudoreference electrode, and a platinum wire auxiliary electrode. Cyclic voltammograms were obtained in freshly distilled CH_3CN (0.1 M *n*-Bu_4NClO_4) with an analyte concentration of 1 mM under an atmosphere of N_2. Under these experimental conditions, the ferrocene/ferrocenium redox couple was observed at + 363 mV versus Ag wire ($\Delta E_p = 88$ mV) with $i_{pa}/i_{pc} = 0.97$. To obtain the potentials quoted herein (vs SCE), the measured potentials were scaled on the basis of the Fc/Fc^+ potential in CH_3CN (0.1 M *n*-Bu_4NClO_4) versus SCE (+ 380 mV).[12] EPR spectra were obtained by using a Bruker ESP-300E spectrometer fitted with a liquid helium cooled probe. Mass spectrometry data for metal complexes were obtained at the Mass Spectrometry Facility, Department of Chemistry, University of California, Riverside. Elemental analyses were performed by Atlantic Microlabs of Norcross, GA.

Caution! Perchlorate salts of metal complexes with organic ligands are potentially explosive. Only small amounts of material should be prepared, and these should be handled with great care.[13]

Synthesis of Ligands. *N*,*N*-Bis((6-phenyl-2-pyridyl)methyl)-*N*-((2-pyridyl)methyl)amine (6-Ph_2TPA) was synthesized following, in part, reported literature procedures.[6a] 6-Phenyl-2-pyridinecarboxyaldehyde was prepared from 6-bromopicolylaldehyde following a method reported by Canary and co-workers.[6a] Modified procedures are reported for the synthesis of 6-phenyl-2-pyridinemethanol and 2-(chloromethyl)-6-phenylpyridine hydrochloride.

6-Phenyl-2-pyridinemethanol. To a methanol solution (40 mL) of 6-phenyl-2-pyridinecarboxyaldehyde (3.37 g, 18.4 mmol) was added dropwise an aqueous solution (15 mL) of $NaBH_4$ (0.974 g, 25.8 mmol) over a period of 5 min. The resulting solution was stirred at ambient temperature for ∼30 min. It was then heated at ∼50 °C for 2 h. To the cooled solution was added 6 M HCl to pH = 1, and this solution was stirred for ∼5 min. To this solution was added 1 M NaOH to pH = 12. The resulting solution was extracted with methylene chloride (3 × 80 mL), and the combined organic fractions were dried over Na_2SO_4. Filtration and evaporation of the solvent under reduced pressure yielded a yellow oil (3.39 g, 99%). ^1H NMR ($CDCl_3$, 400 MHz) δ 8.02−7.98 (m, 2H), 7.73 (t, J = 7.7 Hz, 1H), 7.62 (d, J = 7.7 Hz, 1H), 7.49−7.39 (m, 3H), 7.14 (d, J = 7.7 Hz, 1H), 4.80 (s, 2H). These ^1H NMR spectroscopic features matched those previously reported.[6a]

2-(Chloromethyl)-6-phenylpyridine hydrochloride. To a 250-mL round-bottom flask containing 6-phenyl-2-pyridinemethanol (3.39 g, 18.3 mmol) in an ice bath was added dropwise 20 mL of freshly distilled thionyl chloride. After an initial vigorous reaction subsided, the reaction mixture was refluxed for 2 h. It was then allowed to cool, and unreacted $SOCl_2$ was removed under reduced pressure. The resulting solid was collected, washed several times with CH_2Cl_2, and dried, yielding a white powder (3.95 g, 90%). ^1H NMR (CD_3CN, 400 MHz) δ 8.28 (t, J = 8.0 Hz, 1H), 8.12−8.09 (m, 2H), 8.00 (d, J = 8.0 Hz, 1H), 7.81 (d, J = 8.0 Hz, 1H),

(3) (a) Tanner, A.; Bowater, L.; Fairhurst, S. A.; Bornemann, S. *J. Biol. Chem.* **2001**, *47*, 43627−43634. (b) Tanner, A.; Bornemann, S. *J. Bacteriol.* **2000**, *182*, 5271−5273.
(4) (a) Dai, Y.; Pochapsky, T. C.; Abeles, R. H. *Biochemistry* **2001**, *40*, 6379−6387. (b) Al-Mjeni, F.; Ju, T.; Pochapsky, T. C.; Maroney, M. J. *Biochemistry* **2002**, *41*, 6761−6769.
(5) Creighton, D. J.; Hamilton, D. S. *Arch. Biochem. Biophys.* **2001**, *387*, 1−10.
(6) (a) Chuang, C.-L.; Lim, K. T.; Chen, Q.; Zubieta, J.; Canary, J. W. *Inorg. Chem.* **1995**, *34*, 2562−2568. (b) Chuang, C.-L.; Lim, K. T.; Canary, J. W. *Supramol. Chem.* **1995**, *5*, 39−43.
(7) (a) Mandon, D.; Machkour, A.; Goetz, S.; Welter, R. *Inorg. Chem.* **2002**, *41*, 5364−5372. (b) Mandon, D.; Nopper, A.; Litrol, T.; Goetz, S. *Inorg. Chem.* **2001**, *40*, 4803−4806.
(8) (a) Jensen, M. P.; Lange, S. J.; Mehn, M. P.; Que, E. L.; Que, L., Jr. *J. Am. Chem. Soc.* **2003**, *125*, 2113−2128. (b) Lange, S. J.; Miyake, H.; Que, L., Jr. *J. Am. Chem. Soc.* **1999**, *121*, 6330−6331.
(9) He, Z.; Craig, D. C.; Colbran, S. B. *J. Chem. Soc., Dalton Trans.* **2002**, 4224−4235.
(10) Armarego, W. L. F.; Perrin, D. D. *Purification of Laboratory Chemicals*; 4th Ed.; Butterworth-Heinemann: Boston, MA, 1996.
(11) Evans, D. F. *J. Chem. Soc.* **1959**, 2003−2005.
(12) Connelly, N. G.; Geiger, W. E. *Chem. Rev.* **1996**, *96*, 877−910.
(13) Wolsey, W. C. *J. Chem. Educ.* **1973**, *50*, A335−A337.

7.61−7.56 (m, 3H), 5.28 (s, 2H). These ^{1}H NMR spectroscopic features matched those previously reported.[6a]

***N*,*N*-Bis((6-phenyl-2-pyridyl)methyl)-*N*-((2-pyridyl)methyl)-amine (6-Ph$_2$TPA).** This ligand has been previously reported.[6b,7a] However, the preparative method we have employed has not been reported. A 250-mL round-bottom flask was charged with 2-(chloromethyl)-6-phenylpyridine hydrochloride (6.62 g, 27.6 mmol), 2-pyridylmethylamine (1.49 g, 13.8 mmol), sodium carbonate (7.3 g), tetrabutylammonium bromide (∼3 mg), and CH_3CN (300 mL). After establishing a nitrogen atmosphere, the mixture was refluxed for 20 h. The reaction mixture was then cooled to room temperature and poured into 1 M NaOH (∼150 mL). The resulting solution was extracted with methylene chloride (3 × 150 mL), and the combined organic fractions were dried over Na_2SO_4. After filtration, the organic solution was brought to dryness under reduced pressure. Column chromatography on silica gel (230−400 mesh; 1:2 methanol/ethyl acetate, $R_f \approx 0.8$), followed by removal of the solvent under reduced pressure, yielded a white solid material (4.59 g, 75%). Mp: 103−105 °C. ^{1}H NMR (CD_3CN, 400 MHz) δ 8.49 (d, J = 4.8 Hz, 1H), 8.06−8.02 (m, 4H), 7.77 (t, J = 7.7 Hz, 2H), 7.72−7.67 (m, 4H), 7.56 (d, J = 7.6 Hz, 2H), 7.49−7.40 (m, 6H), 7.20−7.18 (m, 1H), 3.96 (s, 6H); (CD_3OD, 400 MHz) δ 8.42 (d, J = 4.4 Hz, 1H), 7.96 (d, J = 7.2 Hz, 4H), 7.77 (t, J = 7.1 Hz, 4H), 7.64 (d, J = 7.6 Hz, 2H), 7.55 (d, J = 7.6 Hz, 2H), 7.44−7.36 (m, 6H), 7.24−7.22 (m, 1H), 4.01 (s, 2H), 3.99 (s, 4H); ^{13}C-{^{1}H} NMR (CD_3OD, 100 MHz) δ 160.8, 160.5, 158.4, 149.6, 140.8, 138.9, 138.8, 130.1, 129.8, 128.3, 125.0, 123.9, 123.1, 120.5, 61.5, 61.4 (16 signals expected and observed). LREI-MS *m*/*z* (relative intensity): 443 ([M + H]$^+$, 100%). Anal. Calcd for $C_{30}H_{26}N_4$: C, 81.41; H, 5.93; N, 12.67. Found: C, 81.18; H, 5.93; N, 12.71.

6-(3,5-Dimethylphenyl)-2-pyridinecarboxyaldehyde. To a stirred solution of 6-bromopicolylaldehyde[14] (3.01 g, 16.2 mmol) and Pd(PPh$_3$)$_4$ (0.561 g, 0.485 mmol) in 30 mL of toluene under nitrogen were added 17 mL of 2 M Na_2CO_3(aq) and 3,5-dimethylphenylboronic acid (2.91 g, 19.4 mmol) in 15 mL of methanol. The resulting mixture was refluxed for 12 h. It was then allowed to cool and was partitioned between 100 mL of methylene chloride and 60 mL of 2 M Na_2CO_3(aq) containing 6 mL of concentrated NH_3. The organic layer was dried over Na_2SO_4, filtered, and brought to dryness under reduced pressure. Column chromatography on silica gel (230−400 mesh; 4:1 ethyl acetate/hexanes, $R_f \approx 0.6$) followed by removal of the solvent under reduced pressure yielded yellow solid material (3.00 g, 88%). ^{1}H NMR ($CDCl_3$, 270 MHz) δ 10.1 (s, 1H), 8.10−7.60 (m, 2H), 7.85 (d, J = 7.2 Hz, 1H), 7.76 (s, 2H), 7.15 (s, 1H), 2.40 (s, 6H); ^{13}C{^{1}H} NMR ($CDCl_3$, 100 MHz) δ 194.1, 158.3, 152.7, 138.6, 138.3, 137.7, 131.4, 124.9, 124.7, 119.7, 21.5 (11 signals expected and observed).

6-(3,5-Dimethylphenyl)-2-pyridinemethanol. This was prepared following the procedure for 6-phenyl-2-pyridinemethanol. Yield 2.99 g, 99%. ^{1}H NMR (CD_3CN, 270 MHz) δ 7.80 (t, J = 7.7 Hz, 1H), 7.71−7.68 (m, 3H), 7.32 (d, J = 7.6 Hz, 1H), 7.09 (bs, 1H), 4.69 (d, J = 5.6 Hz, 2H), 3.76, (t, J = 5.6 Hz), 2.37 (s, 6H); ^{13}C-{^{1}H} NMR (CD_3CN, 67.5 MHz) δ 161.5, 157.1, 140.0, 139.3, 138.9, 138.6, 131.5, 125.6, 119.8, 65.4, 21.5 (11 signals expected and observed). LREI-MS *m*/*z* (relative intensity): 212 ([M − H]$^+$, 100%).

2-(Chloromethyl)-6-(3,5-dimethylphenyl)pyridine hydrochloride. This was prepared following the procedure for 2-(chloromethyl)-6-phenylpyridine hydrochloride. Yield 3.63 g, 97%. ^{1}H NMR (CD_3OD, 400 MHz) δ 8.69 (t, J = 8.0 Hz, 1H), 8.31 (d, J = 8.0 Hz, 1H), 8.17 (d, J = 7.8 Hz, 1H), 7.61 (bs, 2H), 7.36 (s, 1H), 5.20 (s, 2H), 2.46 (s, 6H); ^{13}C{^{1}H} NMR (CD_3OD, 100 MHz) δ 155.7, 153.2, 149.3, 141.1, 135.3, 132.0, 127.6, 127.4, 126.9, 41.2, 21.5 (11 signals expected and observed).

***N*,*N*-Bis((6-(3,5-dimethyl)phenyl-2-pyridyl)methyl)-*N*-((2-pyridyl)methyl)amine (6-(Me$_2$Ph)$_2$TPA).** This was prepared following the procedure for 6-Ph$_2$TPA. Yield 5.00 g, 70%. ^{1}H NMR (CD_3CN, 400 MHz) δ 8.47 (m, 1H), 7.75−7.55 (m, 10H), 7.50 (d, J = 7.6 Hz, 1H), 7.18−7.14 (m, 1H), 7,02 (bs, 2H), 3.90 (s, 6H), 2.30 (s, 6H); ^{13}C{^{1}H} NMR (CD_3CN, 100 MHz) δ 160.7, 160.3, 157.3, 149.9, 140.3, 139.2, 138.2, 137.3, 131.4, 125.6, 123.9, 123.0, 122.3, 119.5, 61.0, 60.9, 21.6 (17 signals expected and observed). LREI-MS *m*/*z* (relative intensity): 499 ([M + H]$^+$, 55%). Anal. Calcd for $C_{28}H_{26}N_4 \cdot 0.5H_2O$: C, 80.43; H, 6.95; N, 11.04. Found: C, 80.30; H, 6.80; N, 10.99. ^{1}H NMR in dry CD_3CN confirmed the presence of water in the elemental analysis sample.

General Procedure for Synthesis of Metal Complexes. To a methanol slurry (2 mL) of the ligand (6-Ph$_2$TPA or 6-(Me$_2$Ph)$_2$TPA) was added a methanol solution (2 mL) of M(ClO$_4$)$_2$·6H$_2$O (M = Mn, Co, Ni, or Zn; <100 mg scale), and the resulting mixture was stirred at ambient temperature until all of the ligand had dissolved (∼15 min) and then for an additional 20 min. Each solution was then added to excess diethyl ether (∼80 mL), and the resulting cloudy solution was cooled at ∼−20 °C for 12 h. Solid that had deposited in each reaction mixture was then collected and carefully dried under vacuum.

[(6-Ph$_2$TPA)Mn(CH$_3$OH)$_3$](ClO$_4$)$_2$ (1). Recrystallization of a pale yellow-brown solid from diethyl ether diffusion into a CH_3OH solution yielded two types of crystals (light brown, **1A**; and colorless, **1B**), both suitable for single crystal X-ray diffraction (combined yield: 57%). LRFAB-MS (CH_3CN/NBA), *m*/*z* (relative intensity): 596 ([M − ClO$_4$ − 3CH$_3$OH]$^+$, 100%). Anal. Calcd for $C_{30}H_{26}N_4Cl_2O_8Mn(CH_3OH)_{1.5}$: C, 50.87; H, 4.34; N, 7.54. Found: C, 50.57; H, 3.98; N, 7.72. By X-ray crystallography, three methanol molecules are coordinated to the Mn(II) center in this complex. An additional one or two methanol solvate molecules, respectively, were also found in the two different crystalline forms of this complex (**1A·CH$_3$OH** and **1B·2CH$_3$OH**) that were characterized by X-ray crystallography. Drying of the crystals for elemental analysis indicates that partial loss of methanol will occur under vacuum.

[(6-Ph$_2$TPA)Co(CH$_3$CN)](ClO$_4$)$_2$·CH$_3$CN (2). The deposited purple solid was recrystallized by diethyl ether diffusion into a CH_3OH/CH_3CN (1:1) solution which yielded brown crystalline prisms suitable for single crystal X-ray diffraction (80%). LRFAB-MS (CH_3CN/NBA), *m*/*z* (relative intensity): 600 ([M − ClO$_4$ − CH$_3$CN]$^+$, 57%). Anal. Calcd for $C_{30}H_{26}N_4Cl_2O_8Co(CH_3CN)\cdot CH_3CN$: C, 52.23; H, 4.13; N, 10.76. Found: C, 51.91; H, 4.24; N, 10.97. The presence of a noncoordinated acetonitrile solvate in the solid was confirmed by X-ray crystallography.

[(6-Ph$_2$TPA)Ni(CH$_3$CN)(CH$_3$OH)](ClO$_4$)$_2$ (3). Recrystallization of a light green solid from diethyl ether diffusion into a CH_3OH/CH_3CN (1:1) solution yielded purple crystalline prisms suitable for single crystal X-ray diffraction (70%). LRFAB-MS (CH_3CN/NBA), *m*/*z* (relative intensity): 599 ([M − ClO$_4$ − CH$_3$CN − CH$_3$OH]$^+$, 100%). Anal. Calcd for $C_{30}H_{26}N_4Cl_2O_8Ni(CH_3CN)(CH_3OH)$: C, 51.36; H, 4.31; N, 9.08. Found: C, 50.06; H, 4.23; N, 8.86. Repeated attempts to obtain elemental analysis data for this complex always yielded low carbon contents.

[(6-Ph$_2$TPA)Zn(CH$_3$CN)](ClO$_4$)$_2$ (4). Recrystallization of a white powder from diethyl ether diffusion into a CH_3OH/CH_3CN (1:1) solution yielded colorless crystalline prisms suitable for single crystal X-ray diffraction (72%). LRFAB-MS (CH_3CN/NBA), *m*/*z*

(14) Parks, J. E.; Wagner, B. E.; Holm, R. H. *Inorg. Chem.* **1971**, *10*, 2472−2478.

(relative intensity): 605 ([M − ClO_4 − CH_3CN]$^+$, 100%). ^{1}H NMR (CD_3CN, 270 MHz): δ 8.34 (d, J = 4.6 Hz, 1H), 8.25−8.17 (m, 3H), 7.78 (d, J = 7.6 Hz, 2H), 7.70 (d, J = 7.9 Hz, 2H), 7.61 (d, J = 7.6 Hz, 2H), 7.52 (t, J = 7.3 Hz, 2H), 7.39 (t, J = 7.6 Hz, 4H), 7.12 (d, J = 7.3 Hz, 4H), 4.53 (d, J = 17 Hz, 2H), 4.45 (s, 2H), 4.40 (d, J = 17 Hz, 2H), 1.96 (s, CH_3CN, 3H); ^{13}C{^{1}H} NMR (CD_3CN, 100 MHz) δ 160.7, 157.6, 155.8, 149.1, 143.2, 139.7, 131.4, 130.6, 129.4, 126.9, 126.8, 126.3, 124.5, 57.0, 56.8 (15 of 16 expected signals of the supporting chelate ligand were observed; 1 aromatic resonance was missing, presumably due to overlap with another aromatic signal). Anal. Calcd for $C_{30}H_{26}N_4Cl_2O_8Zn(CH_3CN)\cdot 0.5CH_3CN$: C, 51.73; H, 4.02; N, 10.06. Found: C, 51.68; H, 4.07; N, 10.05. The presence of a noncoordinated acetonitrile solvate in the solid state was confirmed by X-ray crystallography. Drying of the crystals for elemental analysis leads to partial loss of CH_3CN. The amount of CH_3CN present in a dried crystalline sample (1.5 equiv) was confirmed by ^{1}H NMR.

[(6-(Me_2Ph)$_2$TPA)Ni(CH_3CN)$_2$](ClO_4)$_2$ (5). The deposited light green solid was recrystallized by diethyl ether diffusion into a ^{i}PrOH/CH_3CN (1:2) solution, which yielded purple crystalline prisms (68%). LRFAB-MS (CH_3CN/NBA), *m*/*z* (relative intensity): 655 ([M − ClO_4 − 2CH_3CN]$^+$, 100%). Anal. Calcd for $C_{34}H_{34}N_4Cl_2O_8Ni(CH_3CN)_2$: C, 54.53; H, 4.82; N, 10.05. Found: C, 54.63; H, 4.96; N, 10.53.

[(6-(Me_2Ph)$_2$TPA)Zn(CH_3CN)](ClO_4)$_2$ (6). The deposited white powder was recrystallized by diethyl ether diffusion into a CH_3OH/CH_3CN (1:1) solution and yielded colorless crystalline plates suitable for X-ray diffraction (59%). LRFAB-MS (CH_3CN/NBA), *m*/*z* (relative intensity): 661 ([M − ClO_4 − CH_3CN]$^+$, 100%). ^{1}H NMR (CD_3CN, 400 MHz): δ 8.32 (d, J = 5.1 Hz, 1H), 8.22−8.16 (m, 3H), 7.70−7.67 (m, 4H), 7.60 (d, J = 7.7 Hz, 2H), 7.18 (s, 2H), 6.70 (s, 4H), 4.54 (d, 18 Hz, 2H), 4.43 (s; 2H), 4.40 (d, 18 Hz, 2H), 2.19 (s, −CH_3, 6H), 1.96 (s, 3H, CH_3CN); ^{13}C{^{1}H} NMR (CD_3CN, 100 MHz) δ 161.1, 157.5, 155.9, 149.4, 143.2, 143.0, 140.2, 140.0, 132.8, 127.1, 127.0, 126.8, 126.6, 124.5, 56.8, 56.7, 21.6 (17 signals for the 6-(Me_2Ph)$_2$TPA ligand were expected and observed). Anal. Calcd for $C_{34}H_{34}N_4Cl_2O_8Zn(CH_3CN)$: C, 53.92; H, 4.65; N, 8.74. Found: C, 52.72; H, 4.72; N, 8.58. Repeated attempts to obtain elemental analysis data for this complex always led to low carbon contents.

[(TPA)Zn(CH_3CN)](ClO_4)$_2$ (7). The deposited yellow powder was recrystallized by diethyl ether diffusion into a CH_3CN solution and yielded a yellow crystalline solid (84%). LRFAB-MS (CH_3CN/NBA), *m*/*z* (relative intensity): 455 ([M − ClO_4 − CH_3CN]$^+$, 97%). ^{1}H NMR (CD_3CN, 270 MHz): δ 8.79 (d, J = 5.4 Hz, 3H), 8.12 (td, J_1 = 7.7 Hz, J_2 = 1.6 Hz, 3H), 7.68 (t, J = 6.4 Hz, 3H), 7.60 (d, J = 7.9 Hz, 3H), 4.27 (s, 6H); ^{13}C{^{1}H} NMR (CD_3CN, 68 MHz) δ 155.3, 148.5, 142.2, 125.6, 125.1, 57.0 (6 signals for the TPA ligand were expected and observed). Anal. Calcd for $C_{18}H_{18}N_4Cl_2O_8Zn(CH_3CN)$: C, 40.47; H, 3.57; N, 11.81. Found: C, 40.04; H, 3.60; N, 11.75.

General Procedure for Synthesis of Acetohydroxamate Complexes. To a methanol slurry (2 mL) of the ligand (6-Ph_2TPA) was added a methanol solution (2 mL) of an equimolar amount of $M(ClO_4)_2\cdot 6H_2O$ (<100 mg scale), and the resulting mixture was stirred at ambient temperature until all of the ligand had dissolved (∼15 min) and then for an additional 20 min. This solution was then added to a methanol solution (1 mL) of an equimolar amount of $Me_4NOH\cdot 5H_2O$. Following 1 h of stirring, this solution was added to a methanol solution (1 mL) of 1.04−1.07 equiv of acetohydroxamic acid, and the new solution was stirred for 12 h. At this time, the solvent was removed under reduced pressure. The dried solid was then dissolved in CH_2Cl_2 (10 mL) and filtered through a Celite/glass wool plug. The filtrate solution was then evaporated to dryness.

[((6-Ph_2TPA)Mn)$_2$(μ-ONHC(O)CH_3)$_2$](ClO_4)$_2$ (8). Recrystallization of a pale yellow-brown solid from diethyl ether diffusion into a ^{i}PrOH/CH_3CN (1:3) solution yielded colorless crystals suitable for single crystal X-ray diffraction (yield: 80%). Anal. Calcd for $C_{32}H_{30}N_5ClO_6Mn$: C, 57.30; H, 4.51; N, 10.45. Found: C, 56.99; H, 4.67; N, 10.16.

[(6-Ph_2TPA)Co(ONHC(O)CH_3)](ClO_4) (9). The red solid was recrystallized by diethyl ether diffusion into a ^{i}PrOH/CH_3CN (1:2) solution, which yielded red crystalline prisms suitable for single crystal X-ray diffraction (yield: 84%). Anal. Calcd for $C_{32}H_{30}N_5ClO_6Co$: C, 56.96; H, 4.49; N, 10.39. Found: C, 57.12; H, 4.63; N, 10.72.

[(6-Ph_2TPA)Ni(ONHC(O)CH_3)](ClO_4) (10). Recrystallization of a light green solid from diethyl ether diffusion into a CH_3OH/CH_3CN (1:1) solution yielded green crystalline prisms suitable for single crystal X-ray diffraction (yield: 79%). Anal. Calcd for $C_{32}H_{30}N_5ClO_6Ni$: C, 57.05; H, 4.49; N, 10.40. Found: C, 56.94; H, 4.61; N, 10.29.

[(6-Ph_2TPA)Zn(ONHC(O)CH_3)](ClO_4) (11). The yellow solid was recrystallized by diethyl ether diffusion into an ^{i}PrOH/CH_3CN (1:2) solution, which yielded colorless crystalline prisms suitable for X-ray crystallographic analysis (yield: 68%). ^{1}H NMR (CD_3CN, 400 MHz): δ 9.81 (bs, N-*H*, 1H), 8.04 (d, J = 7.6 Hz, 1H), 7.85−7.75 (m, 2H), 7.45−7.20 (m, 16H), 7.18 (d, J = 7.8 Hz, 1H), 4.55 (d, J = 15 Hz, 2H), 4.35 (d, J = 15 Hz, 2H), 4.24 (s, 2H), 1.46 (s, CH_3, 3H); ^{13}C{^{1}H} NMR (CD_3CN, 100 MHz) δ 164.5, 159.6, 156.0, 155.8, 148.5, 141.4, 140.4, 139.5, 130.3, 129.5, 128.8, 125.1, 124.7, 124.2, 123.6, 61.7, 58.2, 17.9 (18 signals expected and observed). Anal. Calcd for $C_{32}H_{30}N_5ClO_6Zn$: C, 56.54; H, 4.45; N, 10.31. Found: C, 56.05; H, 4.53; N, 10.72.

X-ray Crystallography. A crystal of **1A**, **1B**, **2**−**4**, and **6**−**11** was mounted on a glass fiber with traces of viscous oil and then transferred to a Nonius KappaCCD diffractometer with Mo Kα radiation (λ = 0.71073 Å) for data collection at 150(1) K. For each compound, an initial set of cell constants was obtained from 10 frames of data that were collected with an oscillation range of 1 deg/frame and an exposure time of 20 s/frame. Final cell constants for each complex were determined from a set of strong reflections from the actual data collection. For each data set, these reflections were indexed, integrated, and corrected for Lorentz, polarization, and absorption effects using DENZO-SMN and SCALEPAC.[15] The structures were solved by a combination of direct methods and heavy atom using SIR 97. All of the non-hydrogen atoms were refined with anisotropic displacement coefficients. Unless otherwise stated, hydrogen atoms were assigned isotropic displacement coefficients U(H) = 1.2U(C) or 1.5U(Cmethyl), and their coordinates were allowed to ride on their respective carbons using SHELXL97.

Structure Solution and Refinement. Complex **1A·CH_3OH** crystallized in the space group $P2_1/a$. One molecule of noncoordinated methanol is present per asymmetric unit. All hydrogen atoms were located and refined independently using SHELXL97, except those of the noncoordinated molecule of methanol, which were assigned isotropic displacement coefficients. Complex **1B·2CH_3OH** crystallized in the space group $P\bar{1}$. Two noncoordinated molecules of methanol are present in the asymmetric unit. All hydrogen atoms were located and refined independently using SHELXL97, except hydrogen atoms on C(31), C(32), C(33) of the coordinated molecules of methanol, and on C(34), O(12), and C(35)

(15) Otwinowski, Z.; Minor, W. *Methods Enzymol.* **1997**, *276*, 307−326.

of the noncoordinated solvate molecules of methanol, which were assigned isotropic displacement coefficients. Complex **2·2CH$_3$CN** crystallized in the space group $P2_1/c$. Two noncoordinated acetonitrile molecules are present in the asymmetric unit. All hydrogen atoms were located and refined independently using SHELXL97, except those on C(32) of the coordinated molecule of acetonitrile, and on C(34) and C(36) of the noncoordinated molecules of acetonitrile, which were assigned isotropic displacement coefficients. In the structure of **2·2CH$_3$CN**, each perchlorate anion exhibits disorder. Each disordered atom was split into two fragments (O(2)/O(2′), O(3)/O(3′), O(4)/O(4′), O(7)/O(7′), O(8)/O(8′)) and was refined. This refinement led to a 0.88:0.12 ratio in occupancy over two positions. Complex **3·CH$_3$OH** crystallized in the space group $Pca2_1$. The methanol hydroxyl proton of nickel-bound methanol was located and refined independently using SHELXL97. One molecule of noncoordinated methanol is present per asymmetric unit. One perchlorate anion exhibits disorder. Each oxygen atom of this perchlorate (O(6)−O(9)) was split into two fragments (second denoted by a prime) and refined. This refinement led to a 0.50:0.50 ratio in occupancy over two positions for each oxygen atom. Complex **4·2CH$_3$CN** crystallized in the space group $P2_1/c$. Two molecules of noncoordinated acetonitrile solvate are present in the asymmetric unit. All hydrogen atoms were located and refined independently using SHELXL97, except those on C(32) of the coordinated molecule of acetonitrile, and on C(34) and C(36) of the noncoordinated solvate molecules of acetonitrile, which were assigned isotropic displacement coefficients. Each perchlorate anion exhibits disorder. Each disordered oxygen atom was split into two fragments (second denoted by a prime) and was refined. This refinement led to a 0.83:0.17 ratio for O(2), O(3), and O(4) and a 0.92:0.08 ratio for O(7) and O(8). Complex **6·2.5CH$_3$CN** crystallized in the space group $P\bar{1}$. Two formula units are present per asymmetric unit, with the second denoted by "A." Five molecules of noncoordinated acetonitrile were present in the asymmetric unit. Three of the four perchlorate anions exhibit disorder. Each disordered oxygen atom (O(1)−O(4), O(3A), O(4A), O(7), O(8)) was split into two fragments (second denoted by a prime) and refined. This refinement led to a 0.83:0.17 ratio in occupancy over two positions for each oxygen atom. Complex **7·CH$_3$CN** crystallized in the space group $P2_1/a$. One molecule of noncoordinated CH_3CN was found in the lattice. All hydrogen atoms were located and refined independently using SHELXL97. Complex **8·0.75-CH$_3$CN·0.75Et$_2$O** crystallizes in the space group $P\bar{1}$ with two formula units present per asymmetric unit, with the second denoted by "A". One perchlorate anion exhibits disorder in the positions of the chlorine atom and three oxygen atoms. Each was split into two fragments and refined. This refinement led to a 0.50:0.50 ratio in occupancy over two positions for each atom. One full molecule of acetonitrile solvate was identified. Another half-occupied acetonitrile molecule, as well as two diethyl ether molecules, one of which is half-occupied, were also identified. Complex **9** crystallized in the space group $P2_1/c$. All hydrogen atoms were located and refined independently using SHELXL97. Complex **10·1.5CH$_3$CN** crystallized in the space group $I2/a$. One and one-half molecules of acetonitrile, dispersed over three half-occupied orientations, were present in the asymmetric unit. All hydrogen atoms were located and refined independently using SHELXL97, except those on C(34), C(36), and C(38) of the noncoordinated molecules of acetonitrile, which were assigned isotropic displacement coefficients. Complex **11** crystallized in the space group $P2_1/n$. All hydrogen atoms were located and refined independently using SHELXL97. All four oxygen atoms of one perchlorate anion exhibited disorder. These disordered oxygen atoms were split into three fragments (second denoted by "A" and third denoted by "B") and were refined. This refinement led to a 0.33:0.33:0.33 ratio in occupancy over three positions for each oxygen atom.

Scheme 1

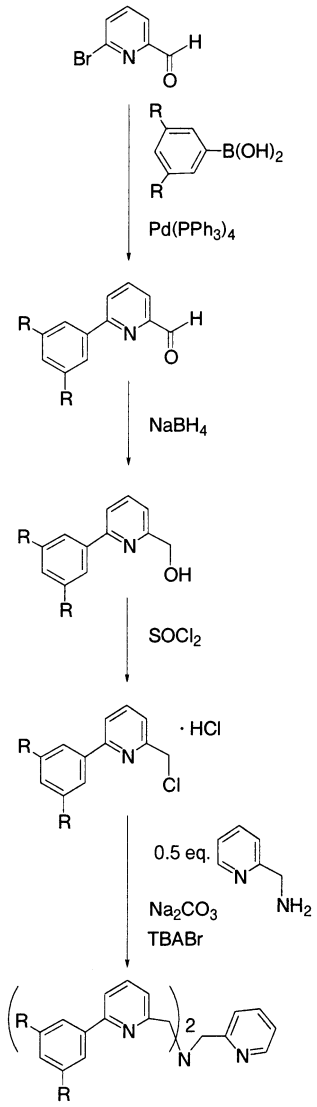

6-Ph$_2$TPA, R = H

6-(Me$_2$Ph)$_2$TPA, R = Me

Results

Synthesis of Ligands. The 6-Ph$_2$TPA and 6-(Me$_2$Ph)$_2$TPA ligands were synthesized following the pathway outlined in Scheme 1. Canary and Mandon et al. have previously reported the synthesis of the 6-Ph$_2$TPA ligand.[7a,6b] In the synthetic pathway reported by Canary et al., the final chelate was produced in 30% yield via a reductive amination reaction involving 6-phenyl-2-pyridinecarboxyaldehyde and 2-aminomethylpyridine in the presence of $NaCNBH_3$. Mandon et al. utilized a Suzuki coupling pathway to prepare 6-Ph$_2$TPA starting from *N*,*N*-bis(6-bromo-2-pyridylmethyl)-*N*-(2-pyridylmethyl)amine and phenylboronic acid. However, no yield was reported for this reaction. We have found that a relatively high yield synthesis (overall yield: 53% starting from 6-bromopicolylaldehyde) of 6-Ph$_2$TPA may be achieved

Scheme 2

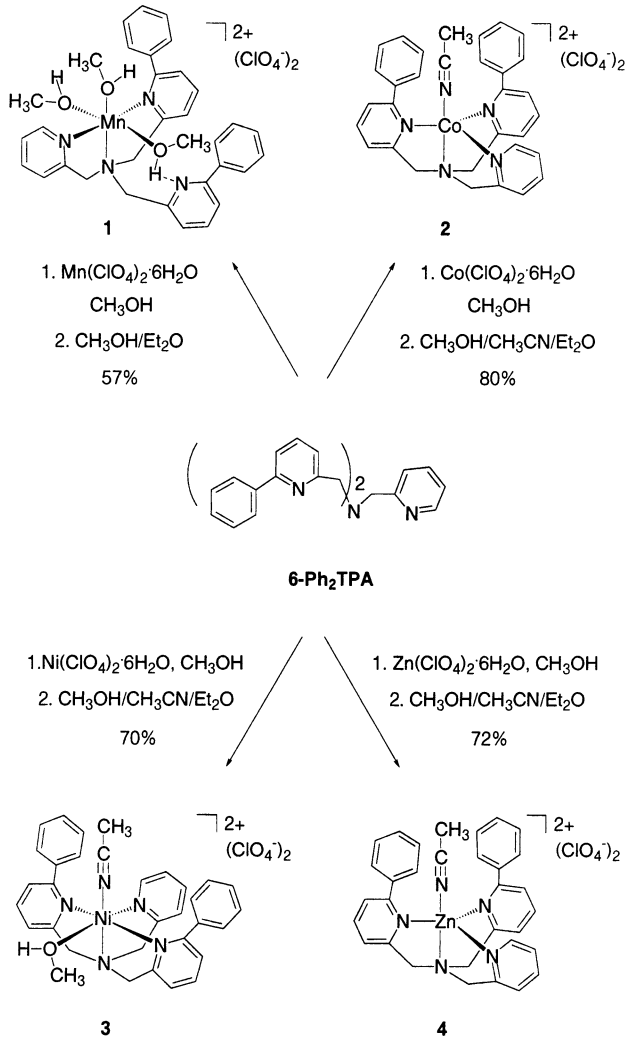

using a synthetic route that involves as the final step alkylation of 2-aminomethylpyridine with 2 equiv of 2-(chloromethyl)-6-phenylpyridine hydrochloride. The crude material obtained from this reaction may be purified by column chromatography on silica gel using methanol as the final eluent. When purified, the 6-Ph_2TPA and 6-$(Me_2Ph)_2$TPA ligands are pale yellow to white solids with moderate to good solubility in several organic solvents (e.g., methylene chloride, acetonitrile, methanol), albeit the methyl derivative 6-$(Me_2Ph)_2$TPA exhibits better solubility, particularly in acetonitrile solution.

Synthesis and Isolation of Divalent Metal Complexes Having Solvent-Occupied Coordination Sites. Treatment of a methanol solution of 6-Ph_2TPA or 6-$(Me_2Ph)_2$TPA with a methanol solution of an equimolar amount of a divalent metal perchlorate salt ($M(ClO_4)_2 \cdot 6H_2O$, M = Mn, Co, Ni, Zn) yielded crude solid materials following precipitation induced by the addition of diethyl ether. Recrystallization of the 6-Ph_2TPA manganese derivative **1** from methanol/ethyl ether yielded a clear crystalline solid. 6-Ph_2TPA-ligated cobalt and nickel perchlorate complexes (**2** and **3**), and a 6-$(Me_2Ph)_2$TPA-ligated zinc perchlorate derivative (**6**), were obtained as crystalline solids from diethyl ether diffusion into methanol/acetonitrile solutions. A 6-Ph_2TPA-chelated

Scheme 3

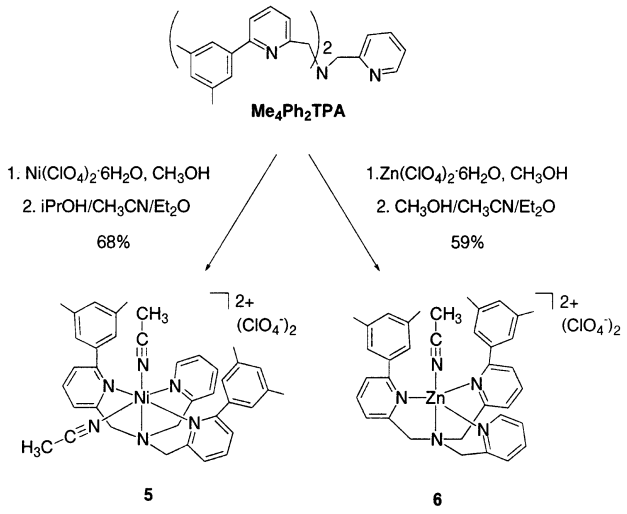

nickel complex (**5**) was obtained as single crystals upon recrystallization from 2-propanol/acetonitrile/diethyl ether. In all cases, yields of analytically pure crystalline materials exceeded 50% (Schemes 2 and 3).

X-ray Structures. Single crystals of X-ray quality were obtained for compounds **1**−**4**, and **6**. Details of the data collection and structure refinement are given in Table 1. Selected bond distances and angles are given in Tables 2 and 3.

[(6-Ph_2TPA)Mn$(CH_3OH)_3$]$(ClO_4)_2$ (1). Crystallization of the Ph_2TPA-ligated Mn(II) complex from methanol/diethyl ether repeatedly produced two crystalline forms of the complex (light brown and colorless crystals) in an approximately 2:1 ratio. The light brown crystals (**1A·CH_3OH**) belong to the monoclinic space group $P2_1/a$ and were found to contain one molecule of noncoordinated methanol in the lattice. The colorless crystalline (**1B·2CH_3OH**) material instead crystallized in the triclinic space group $P\bar{1}$ and was found to contain two noncoordinated methanol molecules per asymmetric unit. As the overall structural features of the cationic portions of **1A·CH_3OH** and **1B·2CH_3OH** are very similar, only a single ORTEP representation of **1B·2CH_3-OH** is shown in Figure 1. In this structure, the Mn(II) ion adopts a distorted octahedral geometry, with the 6-Ph_2TPA ligand binding in a meridional fashion, with only one of the two available phenyl-substituted pyridyl groups binding to the divalent manganese center. This type of coordination is not unexpected as halide-, alkyl-, and aryl-substituted pyridyl donors have been previously shown to exhibit hemilabile behavior with a variety of metal ions.[7,9,16,17] However, reported manganese complexes of TPA and substituted alkyl derivatives have to date shown coordination of all available nitrogen atoms of the tetradentate chelate donor.[18]

The Mn−N distances in **1A·CH_3OH** and **1B·2CH_3OH** are generally similar. However, while identical $M-N_{py}$

(16) 6-Me_3TPA. Fe: (a) Jo, D.-H.; Chiou, Y.-M.; Que, L., Jr. *Inorg. Chem.* **2001**, *40*, 3181−3190. Cu(II): (b) Nagao, H.; Komeda, N.; Mukaida, M.; Suzuki, M.; Tanaka, K. *Inorg. Chem.* **1996**, *35*, 6809−6815.

(17) TPA. Cu(I): Tyeklár, Z.; Jacobson, R. R.; Wei, N.; Murthy, N. N.; Zubieta, J.; Karlin, K. D. *J. Am. Chem. Soc.* **1993**, *115*, 2677−2689.

Table 1. Summary of X-ray Data Collection and Refinement[a]

	1A·CH$_3$OH	**1B·2CH$_3$OH**	**2·2CH$_3$CN**	**3·CH$_3$OH**	**4·2CH$_3$CN**	**6·2.5CH$_3$CN**
empirical formula	$C_{34}H_{42}N_4Cl_2O_{12}Mn$	$C_{35}H_{46}N_4Cl_2O_{13}Mn$	$C_{36}H_{35}N_7Cl_2O_8Co$	$C_{34}H_{37}N_5Cl_2O_{10}Ni$	$C_{36}H_{35}N_7Cl_2O_8Zn$	$C_{41}H_{44.5}N_{7.5}Cl_2O_8Zn$
fw	824.56	856.60	823.54	805.30	829.98	906.61
cryst syst	monoclinic	triclinic	monoclinic	orthorhombic	monoclinic	triclinic
space group	$P2_1/a$	$P\bar{1}$	$P2_1/c$	$Pca2_1$	$P2_1/c$	$P\bar{1}$
a (Å)	13.5366(2)	10.8211(2)	13.6560(3)	20.2150(2)	13.6463(2)	11.18630(10)
b (Å)	16.8549(2)	14.0027(3)	19.2024(4)	14.4727(2)	19.2789(3)	18.4130(2)
c (Å)	17.4487(3)	15.1617(4)	14.2572(3)	12.3174(4)	14.2590(2)	21.6868(4)
α (deg)		96.8521(8)				90.7240(5)
β (deg)	104.9156(5)	107.5620(9)	94.5372(12)		94.5087(5)	90.3750(5)
γ (deg)		110.3167(13)				106.4669(7)
V (Å^3)	3846.92(10)	1988.48(8)	3726.92(14)	3603.65(13)	3739.73(10)	4283.10(10)
Z	4	2	4	4	4	4
d_{calcd}, Mg m^{-3}	1.424	1.431	1.468	1.484	1.474	1.406
temp (K)	150(1)	150(1)	150(1)	150(1)	150(1)	150(1)
cryst size (mm^3)	0.33 × 0.25 × 0.23	0.28 × 0.25 × 0.08	0.28 × 0.25 × 0.13	0.35 × 0.28 × 0.20	0.40 × 0.38 × 0.28	0.30 × 0.15 × 0.10
abs coeff (mm^{-1})	0.547	0.534	0.665	0.751	0.861	0.759
2θ max (deg)	54.94	55.04	54.98	54.96	55.00	55.78
reflns collected	16616	13924	14524	7953	15122	29920
indep reflns	8738	8886	8517	7953	8530	19735
variable params	633	622	616	513	617	1121
R1/wR2[b]	0.0565/0.1464	0.0533/0.1330	0.0511/0.1252	0.0613/0.1468	0.0367/0.0890	0.0532/0.1118
GOF (F^2)	1.030	1.037	1.032	1.119	1.026	1.014
largest diff (e Å^{-3})	0.933/−0.521	1.042/−0.970	0597/−0.434	0.867/−0.586	0.634/−0.575	1.683/−0.851

[a] Radiation used: Mo Kα (λ = 0.71073 Å). Diffractometer: Nonius KappaCCD. [b] $R1 = \sum||F_o| - |F_c||/\sum|F_o|$; $wR2 = [\sum[w(F_o^2 - F_c^2)^2]/[\sum(F_o^2)^2]]^{1/2}$ where $w = 1/[\sigma^2(F_o^2) + (aP)^2 + bP]$.

Table 2. Selected Bond Distances for Solvent-Coordinated Complexes[a]

	1A·CH$_3$OH	**1B·2CH$_3$OH**	**2·2CH$_3$CN**	**3·CH$_3$OH**	**4·2CH$_3$CN**	**6A**[b]	**6B**[b]
M−N(1)	2.254(3)	2.254(2)	2.052(2)	2.065(4)	2.053(2)	2.090(2)	2.072(2)
M−N(2)	2.348(2)	2.355(2)	2.154(2)	2.082(4)	2.167(2)	2.177(2)	2.156(2)
M−N(3)	2.298(2)	2.258(2)	2.082(2)	2.218(5)	2.139(2)	2.113(2)	2.144(2)
M−N(4)			2.114(2)	2.200(5)	2.075(2)	2.064(2)	2.076(2)
M−N(5)			2.059(2)	2.044(4)	2.070(2)	2.073(3)	2.060(3)
M−O(1)	2.170(2)	2.199(2)		2.083(3)			
M−O(2)	2.153(2)	2.136(2)					
M−O(3)	2.138(2)	2.164(2)					

[a] Estimated standard deviations in the last significant figure are given in parentheses. [b] Two independent cations are present in the asymmetric unit of **6·2.5CH$_3$CN**.

Table 3. Selected Bond Angles for Solvent-Coordinated Complexes[a]

	1A·CH$_3$OH	**1B·2CH$_3$OH**	**2·2CH$_3$CN**	**3·CH$_3$OH**	**4·2CH$_3$CN**	**6A**[b]	**6B**[b]
N(5)−M−N(2)			171.55(8)	175.12(19)	170.41(6)	169.53(9)	171.10(10)
O(2)−M−N(2)	163.34(10)	163.82(8)					
N(2)−M−N(1)	74.67(10)	74.47(7)	78.54(8)	83.53(14)	79.92(6)	78.37(9)	79.15(9)
N(2)−M−N(3)	74.46(9)	74.51(7)	77.21(8)	76.80(18)	77.05(6)	77.40(9)	77.60(9)
N(2)−M−N(4)			76.68(8)	82.54(17)	78.78(6)	79.63(9)	79.09(9)
N(2)−M−O(3)	94.14(8)	92.78(7)					
N(2)−M−O(1)	90.86(9)	90.89(7)		92.81(14)			
N(1)−M−N(3)	148.80(9)	148.97(8)	110.04(8)	97.71(16)	122.88(6)	119.44(9)	121.00(9)
N(3)−M−O(1)	87.62.(9)	83.69(7)		84.46(17)			
N(1)−M−O(1)	88.42(10)	96.05(8)		175.17(14)			
O(1)−M−N(4)				91.06(17)			
N(1)−M−N(4)			121.28(8)	85.36(15)	111.08(6)	112.24(9)	112.04(10)
N(3)−M−O(3)	93.25(8)	87.65(7)					
O(3)−M−N(1)	93.36(9)	94.57(8)					
N(3)−M−N(4)			114.88(8)	158.59(16)	114.45(6)	116.55(9)	115.48(9)
O(1)−M−O(3)	174.98(9)	169.35(8)					

[a] Estimated standard deviations in the last significant figure are given in parentheses. [b] Two independent cations are present in the asymmetric unit of **6·2.5CH$_3$CN**.

distances are observed in **1B·2CH$_3$OH** (both 2.254(2) Å), the Mn(1)−N(3) distance (2.258(2) Å) involving the phenyl-substituted pyridyl donor is slightly shorter than the Mn(1)−N(3) distance (2.298(2) Å) in **1A·CH$_3$OH**. The Mn−N_{py} distances for both **1A·CH$_3$OH** and **1B·2CH$_3$OH** are comparable to those found for *trans* pyridyl groups in Mn(II) derivatives of the parent TPA ligand, including [Mn(TPA)(μ-O_2CCH$_3$)]$_2$(TCNQ)$_2$·2CH$_3$CN (2.239(3), 2.227(3) Å; TCNQ = tetracyanoquinodimethane), [Mn(TPA)(TCNQ)(CH$_3$OH)](TCNQ)$_2$·2CH$_3$CN (2.253(4), 2.237(4) Å), [Mn(TPA)(NCS)$_2$]·CH$_3$CN (2.265(3), 2.252(3) Å), [Mn$_2$(TPA)$_2$(CA)](ClO$_4$)$_2$·3H$_2$O (2.231(2), 2.205(2) Å), and [Mn$_2$(TPA)$_2$(CA)](ClO$_4$)$_2$·2CH$_3$CN (2.223(4), 2.290(4) Å; CA = chloroanilate).[18a,b] Notably, manganese(II) catecholate derivatives

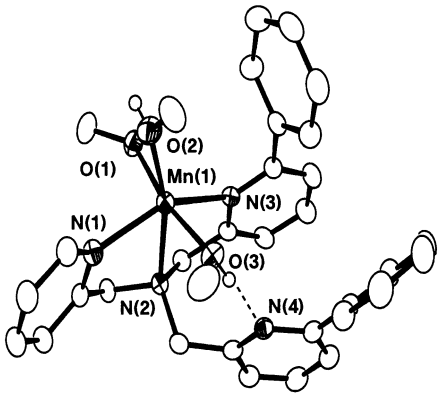

Figure 1. ORTEP representation of the cationic portion of **1B·2CH$_3$OH**. All ellipsoids are drawn at the 50% probability level. All hydrogens except the methanol protons were omitted for clarity.

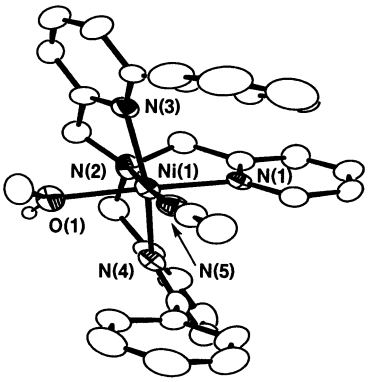

Figure 2. ORTEP representation of the cationic portion of **3·CH$_3$OH**. All ellipsoids are drawn at the 50% probability level. All hydrogens except the methanol proton were omitted for clarity.

of 6-Me$_3$-TPA, in which all the pyridyl donors of the chelate are coordinated to the manganese(II) center, have generally longer *trans* Mn−N$_{py}$ bond distances ([(6-Me$_3$TPA)Mn(DBCH)]ClO$_4$, two cations in the asymmetric unit, 2.367(4), 2.333(5), 2.294(4), 2.368(4) Å; [(6-Me$_3$TPA)Mn(4-NC)]ClO$_4$, 2.316(2), 2.4064(18) Å). This is due to steric crowding involving the 6-methyl substituents on the *trans* pyridyl rings.[18g] On the basis of this literature precedent, it might be anticipated that coordination of the 6-Ph$_2$TPA ligand to a Mn(II) ion in a meridional fashion, with the unsubstituted pyridyl ligand positioned *trans* to a phenyl-substituted pyridyl donor, might result in Mn−N$_{py}$ distances that are elongated relative to those of Mn(II) complexes of the parent TPA ligand. However, as already outlined, this is not the case. This observation, combined with the finding of several interesting secondary interactions involving the ligand (vida infra) in **1**, provides evidence that the 6-Ph$_2$-TPA chelate provides a unique coordination environment on a Mn(II) center relative to that introduced via TPA or 6-Me$_3$-TPA ligation.

In each structure, one of the Mn(II)-bound methanol ligands participates in a CH/π interaction (Figure S1) with the phenyl substituent of the bound pyridyl ring. These interactions are characterized by short C(32)−arene centroid distances (**1A·CH$_3$OH**, 3.44 Å; **1B·2CH$_3$OH**, 3.40 Å) and may be conferred to provide a small amount of stabilization energy (<2 kcal/mol) to the metal-bound alcohol ligand.[19] A secondary hydrogen-bonding interaction involving the same Mn(II)-bound methanol molecule (C(32)−O(2)−H(2A)) and a noncoordinated methanol solvate molecule (**1A·CH$_3$OH**, O(2)···O(12) 2.760(5) Å, O(2)−H(2A)···O(12) 163(4)°; **1B·2CH$_3$OH**, O(2)···O(13) 2.590(4) Å, O(2)−H(2A)···O(13) 156(4)°) is found in the cationic portion of each complex. Notably, a hydrogen-bonding interaction is also found between a different Mn(II)-coordinated methanol molecule (C(33)−O(3)−H(3A)) and the noncoordinated pyridyl nitrogen (**1A·CH$_3$OH**, O(3)···N(4) 2.664(3) Å, O(3)−H(3A)···N(4) 169(3)°; **1B·2CH$_3$OH**, O(3)···N(4) 2.715(3) Å, O(3)−H(3A)···N(4) 174(4)°).

[(6-Ph$_2$TPA)Ni(CH$_3$CN)(CH$_3$OH)](ClO$_4$)$_2$·CH$_3$OH (3·CH$_3$OH). An ORTEP representation of the cationic portion of **3·CH$_3$OH** is shown in Figure 2. The Ni(II) center exhibits an octahedral geometry, with the two phenyl-substituted pyridyl donors bound in a *trans* orientation. The Ni−N$_{py}$ bond lengths for the phenyl-substituted pyridyl donors (Ni−N$_{PhPy}$, 2.200(5), 2.218(5) Å) in **3·CH$_3$OH** are elongated with respect to the unsubstituted pyridyl donor (2.065(4) Å) in the same complex and Ni−N$_{Py}$ distances in a variety of Ni(II) complexes of the parent TPA ligand (av Ni−N$_{py}$ ∼2.08 Å).[20] However, the average Ni−N$_{Py}$ distance in 6-Me$_3$-TPA Ni(II) derivatives (2.215 Å) matches well with the Ni−N$_{PhPy}$ distances in **3·CH$_3$OH**.[21] It is also worth noting that the bond involving the tertiary amine nitrogen in **3·CH$_3$OH** (Ni−N$_{Am}$ 2.082(4) Å) is shorter than that typically found in Ni(II) TPA complexes (av 2.11 Å)[20] but is similar to that found in 6-Me$_3$-TPA complexes (av 2.08 Å).[21] Thus, these structural comparisons indicate that while the 6-Ph$_2$TPA ligand provides additional steric hindrance and hydrophobicity surrounding the divalent nickel center, the geometric parameters of its bonding to Ni(II) generally fall in line with those previously reported for ligands of the tris(pyridylmethyl)-amine family. The same conclusions generally hold for nickel coordination to a recently reported monoaryl-substituted TPA

(18) TPA: (a) Xiang, D. F.; Duan, C. Y.; Tan, X. S.; Liu, Y. J.; Tang, W. X. *Polyhedron* **1998**, *17*, 2647−2653. (b) Oshio, H.; Ino, E.; Mogi, I.; Ito, T. *Inorg. Chem.* **1993**, *32*, 5697−5703. (c) Towle, D. K.; Botsford, C. A.; Hodgson, D. J. *Inorg. Chim. Acta* **1988**, *141*, 167−168. (d) Gultneh, Y.; Farooq, A.; Karlin, K. D.; Liu, S.; Zubieta, J. *Inorg. Chim. Acta* **1993**, *211*, 171−175. 6-Me$_2$TPA: (e) Goodson, P. A.; Oki, A. R.; Hodgson, D. J. *Inorg. Chim. Acta* **1990**, *177*, 59−64. (f) Goodson, P. A.; Oki, A. R.; Glerup, J.; Hodgson, D. J. *J. Am. Chem. Soc.* **1990**, *112*, 6248−6254. 6-Me$_3$TPA: (g) Reynolds, M. F.; Costas, M.; Ito, M.; Jo, D.-H.; Tipton, A. A.; Whiting, A. K.; Que, L., Jr. *JBIC, J. Biol. Inorg. Chem.* **2003**, *8*, 263−272. (h) Zhang, Z.-H.; Bu, X.-H.; Ma, Z.-H.; Bu, W.-M.; Tang, Y.; Zhao, Q.-H. *Polyhedron* **2000**, *19*, 1559−1566.

(19) Nishio, M.; Hirota, M.; Umezawa, Y. *The CH/π Interaction: Evidence, Nature and Consequences*; Wiley-VCH: New York, 1998.

(20) (a) Zhang, Z.-H.; Bu, X.-H.; Zhu, Z.-A.; Jiang, Z.-H.; Chen, Y.-T. *Transition Met. Chem.* **1996**, *21*, 235−237. (b) Ito, M.; Takita, Y. *Chem. Lett.* **1996**, 929−930. (c) Ito, M.; Sakai, K.; Tsubomura, T.; Takita, Y.-S. *Bull. Chem. Soc. Jpn.* **1999**, *72*, 239−247. (d) Tong, B.; Norman, R. E.; Chang, S.-C. *Acta Crystallogr.* **1999**, *C55*, 1236−1238. (e) Tong, B.; Chang, S.-C.; Carpenter, E. E.; O'Connor, C. J.; Lay, J. O., Jr.; Norman, R. E. *Inorg. Chim. Acta* **2000**, *300*, 855−861.

(21) (a) Zhang, Z.-H.; Bu, X.-H.; Ma, Z.-H.; Bu, W.-M.; Tang, Y.; Zhao, Q.-H. *Polyhedron* **2000**, *19*, 1559−1566. (b) Shiren, K.; Ogo, S.; Fujinami, S.; Hayashi, H.; Suzuki, M.; Uehara, A.; Watanabe, Y.; Moro-oka, Y. *J. Am. Chem. Soc.* **2000**, *122*, 254−262.

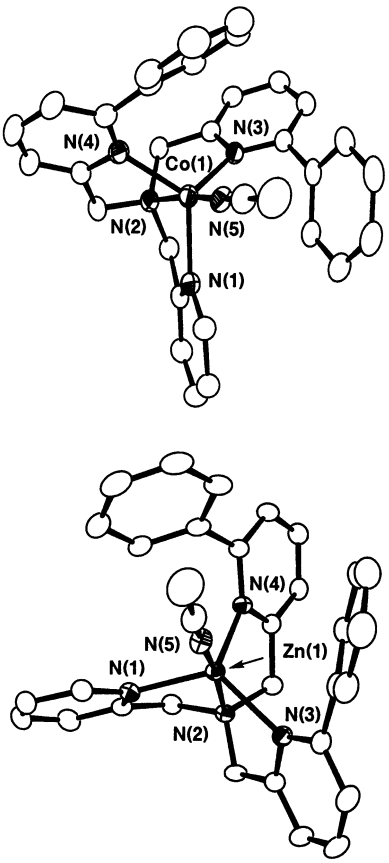

Figure 3. ORTEP representations of the cationic portions of **2·2CH$_3$CN** and **4·2CH$_3$CN**. All ellipsoids are drawn at the 50% probability level. All hydrogens were omitted for clarity.

ligand (*N*-((6-(2′,5′-dimethoxy)phenyl)-(2-pyridyl)methyl)-*N*,*N*-bis((2-pyridyl)methyl)amine).[9]

Notably, the Ni(II)-coordinated acetonitrile molecule in **3·CH$_3$OH** is positioned in a sandwich motif between two phenyl rings of the 6-Ph$_2$TPA ligand. This results in CH/π interactions involving the acetonitrile methyl group and the phenyl rings (Figure S2; C(33)···arene centroid, 3.66, 3.63 Å), as well as in short contacts between the arene carbons and the nitrile carbon (C(32)) and nitrogen (N(5)) of the bound solvent molecule. The presence of the hydrophobic environment has no effect on the Ni−NNCCH$_3$ bond distance (2.044(2) Å), which is identical to that found in [(TPA)Ni(CH$_3$CH$_2$CN)(OH$_2$)](ClO$_4$)$_2$ (2.043(9) Å).[20c]

A series of hydrogen-bonding interactions are present involving the cationic portion of **3·CH$_3$OH** in the solid state. Specifically, the hydroxyl moiety of the coordinate methanol ligand donates a hydrogen bond to a noncoordinated methanol solvate (O(1)···O(10) 2.615(6) Å, O(1)−H(1A)···O(10) 143(5)°), which in turn forms a hydrogen-bonding interaction with a perchlorate anion (O(10)···O(3) 2.816(8) Å).

[(6-Ph$_2$TPA)Co(CH$_3$CN)](ClO$_4$)$_2$·2CH$_3$CN (2·2CH$_3$CN) and [(6-Ph$_2$TPA)Zn(CH$_3$CN)](ClO$_4$)$_2$·2CH$_3$CN (4·2CH$_3$CN). Structurally similar Co(II) and Zn(II) complexes of the 6-Ph$_2$-TPA ligand were isolated and characterized (Figure 3). In each, the metal center adopts a slightly distorted trigonal bipyramidal geometry (**2·2CH$_3$CN**, τ = 0.84; **4·2CH$_3$CN**, τ = 0.79; for a perfect trigonal bipyramid τ = 1),[22] with the three pyridyl nitrogen donors forming the trigonal plane. For each, the divalent metal center is displaced from this plane toward the acetonitrile ligand (**2·2CH$_3$CN**, ∼0.45 Å; **4·2CH$_3$CN**, ∼0.41 Å). The M(II)−N$_{PhPy}$ and M(II)−N$_{py}$ distances in **2·2CH$_3$CN** and **4·2CH$_3$CN** differ by ∼0.02−0.08 Å, with the M(II)−N$_{PhPy}$ distances again being slightly longer. Complex **2·2CH$_3$CN** is the third structurally characterized mononuclear five-coordinate cobalt(II) complex of a TPA-type ligand.[9,23] Notably, one example was isolated using a monoaryl-substituted TPA ligand (*N*-((6-(2′,5′-dimethoxy)phenyl)-(2-pyridyl)methyl)-*N*,*N*-bis((2-pyridyl)-methyl)amine).[9] To our knowledge, four mononuclear, five-coordinate zinc complexes of the parent TPA ligand have been reported.[23a,24] The average Zn−N$_{py}$ bond lengths in these complexes ([(TPA)ZnCl]ClO$_4$,[23a] 2.069 Å; [(TPA)ZnCl]-BPh$_4$·2CH$_3$CN,[24b] 2.073 Å; [(TPA)ZnI]ClO$_4$,[23a] 2.090 Å; [(TPA)Zn(O$_2$CPh)]BPh$_4$·CH$_3$CN,[24b] 2.064 Å) are generally similar to the Zn−N$_{py}$ (2.053(2) Å), and slightly shorter than the average Zn−N$_{PhPy}$ (∼2.11 Å) distances found in **4·2CH$_3$CN**. In the course of our work, we also prepared and characterized [(TPA)Zn(CH$_3$CN)](ClO$_4$)$_2$ (**7·CH$_3$CN**). The geometry of the Zn(II) ion in this complex is more trigonal bipyramidal (τ = 0.97; Figure S3)[22] than is observed for **4·2CH$_3$CN**. Comparison of the bond angles in **4·2CH$_3$CN** and **7·CH$_3$CN** reveals a smaller N$_{amine}$−Zn− N(CH$_3$CN) angle in **4·2CH$_3$CN** (170.41(6)°) than is found in **7·CH$_3$CN** (177.38(7)°). This appears to be a consequence of steric crowding due to the presence of the phenyl substituents, as the bound acetonitrile ligand is canted away from the phenyl-substituted pyridyl donors. The Zn−N distances in **4·2CH$_3$CN** and **7·CH$_3$CN** are generally similar, albeit one Zn−N$_{PhPy}$ bond is elongated in **4·2CH$_3$CN** (Zn(1)−N(3) 2.139(2) Å).

Secondary CH/π interactions involving the bound acetontrile ligand and the 6-Ph$_2$TPA phenyl groups are present in the solid state structures of **2·2CH$_3$CN** and **4·2CH$_3$CN** (Figures S4 and S5).[19] The C(32)···arene centroid distances (**2·2CH$_3$CN**, 3.79, 3.80 Å; **4·2CH$_3$CN**, 3.78, 3.78 Å) are longer than those observed in **3·CH$_3$OH** (vida supra).

In order to evaluate the effect of aryl group substitution on the steric properties of divalent metal complexes, the 6-(Me$_2$Ph)$_2$TPA-ligated **6·2.5CH$_3$CN** (Figure 4) was characterized by X-ray crystallography. Two independent molecules are present in the asymmetric unit. Both cations exhibit a distorted trigonal bipyramidal geometry (τ = 0.83, 0.84),[22] with bond distances, angles, and metrical parameters of secondary CH/π interactions very similar to those of **4·**

(22) Addison, A. W.; Rao, T. N.; Reedijk, J.; van Rijn, J.; Verschoor, G. C. *J. Chem. Soc., Dalton Trans.* **1984**, 1349−1356.
(23) (a) Allen, C. S.; Chuang, C.-L.; Cornebise, M.; Canary, J. W. *Inorg. Chim. Acta* **1995**, *239*, 29−37. (b) Hilt, G.; Jarbawi, T.; Heineman, W. R.; Steckhan, E. *Chem. Eur. J.* **1997**, *3*, 79−88. (c) Nanthakumar, A.; Fox, S.; Murthy, N. N.; Karlin, K. D. *J. Am. Chem. Soc.* **1997**, *119*, 3898−3906.
(24) (a) Canary, J. W.; Allen, C. S.; Castagnetto, J. M.; Chiu, J. M.; Chiu, Y.-H.; Toscano, P. J.; Wang, Y. *Inorg. Chem.* **1998**, *37*, 6255−6262. (b) Adams, H.; Bailey, N. A.; Fenton, D. E.; He, Q.-Y. *J. Chem. Soc., Dalton Trans.* **1997**, 1533−1539. (c) Canary, J. W.; Allen, C. S.; Castagnetto, J. M.; Wang, Y. *J. Am. Chem. Soc.* **1995**, *117*, 8484−8485.

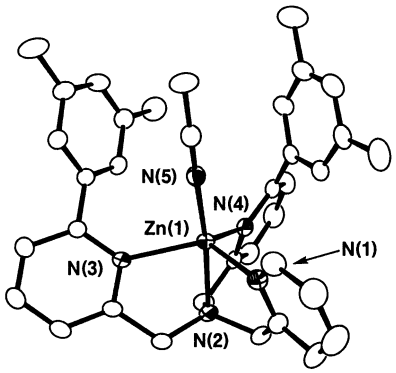

Figure 4. ORTEP representation of one of two cations present in the asymmetric unit of **6·2.5CH$_3$CN**. All ellipsoids are drawn at the 50% probability level. All hydrogens were omitted for clarity.

2CH$_3$CN. Hence, 3,5-dimethyl substitution of the phenyl substituent induces little change in the structural properties of zinc complexes.

Solution Characterization. Electrochemistry. Cyclic voltammetric examination of complexes **1**−**3** and **5** was performed in freshly distilled CH_3CN under an atmosphere of N_2. Complexes **2**, **3**, and **5** exhibit reversible couples corresponding to reduction of the +2 metal complexes, presumably to +1 (Figure S6). The observed formal potentials (scaled to the SCE potential) for these couples are shown in Table 3. The Co(II) complex **2** has a quasireversible Co(II)/Co(I) couple at −1101 mV versus SCE measured at a scan rate of 250 mV/s. The reversibility of this couple decreased at slower scan rates, indicating that the electrochemically generated Co(I) complex can readily react in solution, either with trace O_2 or perhaps with the solvent. No oxidative couples (Co(II)/Co(III)) were observed. Both Ni(II) complexes (**3** and **5**) exhibited very similar electrochemical behavior. Complex **3** has a quasireversible Ni(II)/Ni(I) couple at −881 mV versus SCE, measured at a scan rate of 100 mV/s. Likewise, complex **5** has a quasireversible Ni(II)/Ni(I) couple at −885 mV versus SCE, also measured at a scan rate of 100 mV/s. Thus, while the electrochemically generated Ni(I) complexes are strongly reducing, they are readily observed in thoroughly deoxygenated solutions. The peak-to-peak separations, which are of a similar magnitude as that of the ferrocene/ferrocenium couple, suggest that only minor structural reorganizations accompany the Ni(II)/Ni(I) redox processes. No oxidative couples (Ni(II)/Ni(III)) were observed. The Mn(II) complex **1** is unique in this series, in that no oxidative (Mn(III)/Mn(II)) or reductive (Mn(II)/Mn(I)) couples were observed over the potential range +1.8 V to −1.8 V versus SCE. A weak, quasireversible couple was observed at ∼ −1.25 V. However, the intensity of this feature did not scale with the amount of complex present in solution. Therefore, we suspect that this couple is a result of a trace impurity in the original sample.

Magnetic Moment. The solution magnetic moments of **1**−**3** and **5** (Table 4) were determined at 298 K by the Evans method.[11] The experimentally measured magnetic moment for **1** (6.1 μ_B) is near the spin-only value expected for a high-spin Mn(II) ion (5.9 μ_B), whereas the values found for **2** (4.3 μ_B), **3** (3.2 μ_B), and **5** (3.2 μ_B) are higher than the spin-only values for high-spin Co(II) and Ni(II) (3.9 and 2.8 μ_B, respectively) due to spin−orbit coupling.[25]

Table 4. Selected Physical Properties of **1**−**3** and **5**

	1	**2**	**3**	**5**
UV−vis, nm		477 (105)	558 (10)	556 (10)
(ϵ, M^{-1} cm^{-1})		570 (90)	1007 (15)	1005 (15)
		678 (24)		
CV,[a] mV		−1101	−881	−885
μ_{eff},[b] μ_B	6.1	4.3	3.2	3.2

[a] Potentials reported versus SCE. [b] Average value of two independent determinations at 298 K.

UV−Vis Spectroscopy. Electronic absorption spectra of **2**, **3**, and **5** were recorded in dry CH_3CN solution (Table 4). All spectra show strong ligand-based absorptions at <400 nm. The cobalt complex **2** exhibits three electronic transitions (477(105), 570(90), and 678(24) nm), with extinction coefficients for these transitions suggesting that the Co(II) center in **2** remains five coordinate in CH_3CN solution. On this basis, the transitions corresponding to these absorptions may be assigned as $^4A_2'(F)\rightarrow{}^4E''(P)$, $^4A_2'(F)\rightarrow{}^4A_2'(P)$, and $^4A_2'(F)\rightarrow{}^4E'(F)$, respectively.[26] For the Ni(II) complex **3**, two absorptions are found in the region 400−1100 nm, which correspond to the $^3A_{2g} \rightarrow {}^3T_{1g}(F)$ and $^3A_{2g} \rightarrow {}^3T_{2g}(F)$ transitions, respectively, for an octahedral Ni(II) center. The energy of these absorptions is not affected by methyl substitution in **5** (Table 4).

EPR and ^{1}H NMR Spectroscopy. Mn(II) complex **1** exhibits an axial EPR signal at $g \sim 2.0$, with a six line hyperfine pattern (Figure S7), and $A_{||} = 97 \pm 4$ G.

The ^{1}H NMR spectra of the zinc complexes **4** and **6** in CD_3CN solution at ambient temperature have signals consistent with the X-ray crystallographically determined structures of these complexes, albeit an upfield shifted resonance for the bound acetonitrile molecule involved in a CH/π interaction in each complex is not observed. This is likely due to exchange of the bound CH_3CN with CD_3CN. To probe for CH/π interactions in solution, **4** and **6** were dissolved in CD_3NO_2 and ^{1}H NMR spectra were again obtained. In this case, for **4**, two resonances associated with CH_3CN were found at 2.21 and 1.78 ppm, respectively, each integrating to approximately three protons. Free CH_3CN in CD_3NO_2 is found at 2.00 ppm. Thus, it appears that one of the acetonitrile molecules present in CD_3NO_2 solutions of **4** is shifted upfield, consistent with its involvement in a CH/π interaction. The magnitude of the upfield shift ($\delta = 0.22$ ppm) is smaller than that observed for acetonitrile in CCl_4 versus benzene solution ($\delta = 0.97$ ppm).[19] This may be due to an additional inductive effect resulting from zinc coordination of the acetonitrile molecule in **4**, which would be expected to produce a downfield shift of the CH_3CN resonance. The second CH_3CN resonance found in the ^{1}H NMR spectrum of **4** in CD_3NO_2 is shifted downfield of free acetonitrile by ∼0.21 ppm. In the X-ray structure of **4**, a noncoordinated CH_3CN molecule is present. We propose that

(25) Jolly, W. L. *The Synthesis and Characterization of Inorganic Compounds*; Waveland Press: Prospect Heights, IL, 1970.
(26) Lever, A. B. P. *Inorganic Electronic Spectoscopy*, 2nd ed.; Elsevier: Amsterdam, 1984.

in CD_3NO_2 solution, where the solvent is only a very weak Lewis base, the previously noncoordinating CH_3CN solvate molecule may interact with the zinc center in a sixth coordination position. Formation of a six-coordinate TPA-ligated zinc center has been previously reported.[27] In general, the CD_3NO_2 solution properties of **6** are similar to those of **4**, with an upfield-shifted peak present at 1.82 ppm. The assignment of the upfield shifted resonances at ~1.8 ppm in both **4** and **6** as a bound CH_3CN molecule participating in a CH/π interaction is further supported by comparison of the solution properties of these complexes with those of $[(TPA)Zn(CH_3CN)](ClO_4)_2$ (**7**). Unlike the complexes of the 6-Ph_2TPA and 6-$(Me_2Ph)_2$TPA ligands, **7** does not exhibit an upfield shifted CH_3CN resonance in CD_3NO_2 solution, consistent with the fact that CH/π interactions are not present. A resonance at ~2.12 ppm is observed indicating the presence of a zinc-bound CH_3CN molecule.[28]

Preparation of Hydroxamate Compounds. To evaluate whether using the 6-Ph_2TPA ligand will enable the isolation of mononuclear divalent metal complexes having a chelate anionic ligand, we have investigated the chemistry of divalent metal hydroxamate derivatives. Treatment of the 6-Ph_2TPA ligand with equimolar amounts of $M(ClO_4)_2 \cdot 6H_2O$, $Me_4NOH \cdot 5H_2O$, and acetohydroxamic acid in methanol (Scheme 4) yielded the hydroxamate complexes **8**−**11** in yields of 68−84% as crystalline solids from either $CH_3CN/^iPrOH/Et_2O$ (**8**, **9**, and **11**) or $CH_3CN/MeOH/Et_2O$ (**10**) solutions.

X-ray Crystallography. Details of the data collection and structure refinement are given in Table 5. Selected bond distances and angles are given in Table 6.

$[(6\text{-}Ph_2TPAMn)_2(\mu\text{-}ONHC(O)CH_3)_2](ClO_4)_2 \cdot 0.75CH_3CN \cdot 0.75Et_2O$ ($8 \cdot 0.75CH_3CN \cdot 0.75Et_2O$). To our knowledge, this complex represents the first structurally characterized manganese(II) hydroxamate complex.[29] Two chemically similar, but structurally unique, dimeric cations are found in the asymmetric unit of this complex. As the metrical parameters of these two cations are generally similar, for the most part only one (**8A**; Figure 5) will be discussed. The two manganese centers in the cationic portion of **8A** are bridged by two hydroxamate ligands, with each coordinating in a μ-η^1:η^2-$ONHC(O)CH_3$ fashion. This coordination mode has been previously observed in dimeric Ni(II), Zn(II), and Co(II) hydroxamate complexes.[30−32] The 6-Ph_2TPA ligand chelates to each Mn(II) ion in **8A** in a facial arrangement, with only one of the two available phenyl-substituted pyridyl donors for each 6-Ph_2TPA moiety binding to a Mn(II) center. The facial coordination mode of 6-Ph_2TPA in **8A** and **8B** differs from the meridional type ligation found for the same chelate ligand in **1A·CH₃OH** and **1B·2CH₃OH**. The Mn−N bond distances in both ligand coordination modes are similar (~2.25−2.40 Å), with the Mn−N(amine) distance being the longest for each Mn(II) center. As in **1A·CH₃OH**, the Mn−N_{py} distances for both the phenyl-substituted and unsubstituted pyridyl rings are similar. The average Mn(II)−O distance in **8A** is 2.18 Å (**8B**, 2.18 Å), and the Mn···Mn distance is 3.409 Å (**8B**, 3.386 Å). In **8A**, a relatively weak hydrogen-bonding interaction is found between a hydroxamate N−*H* and a nitrogen atom of one of the two noncoordinated pyridyl donors in the dimer (N(10)···N(4) 3.009(6) Å, N(10)−H···N(4) 139.8°). The other bound

Scheme 4. Synthetic Route for Preparation of Hydroxamate Complexes **8**-**11**[a]

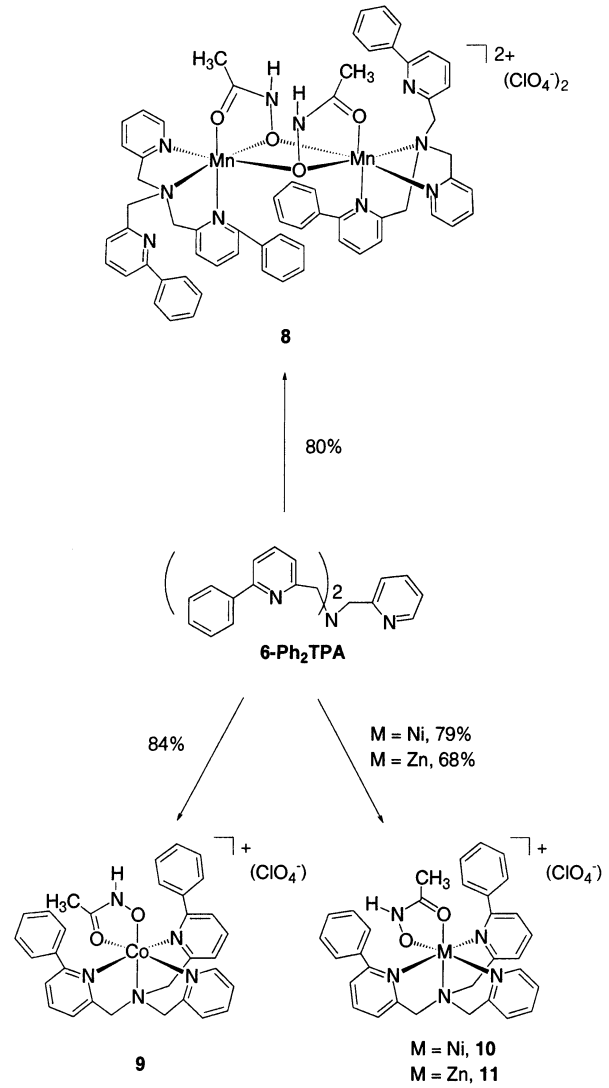

[a] All reactions involve treatment of 6-Ph_2TPA with equimolar amounts of $M(ClO_4)_2 \cdot 6H_2O$, $Me_4NOH \cdot 5H_2O$, and acetohydroxamic acid.

(27) Murthy, N. N.; Karlin, K. D. *J. Chem. Soc., Chem. Commun.* **1993**, 1236−1238.

(28) A downfield-shifted resonance for water is also present in ^{1}H NMR spectra of bulk samples of **7**. Upon heating of the NMR sample at ~45−50° under vacuum for 12 h, the acetonitrile resonance disappears, but the water resonance remains. This indicates that water coordination is also likely in this complex.

(29) Mn(II) complexes of aminohydroxamic acids have been previously reported to form in water solution but were not structurally characterized: Enyedy, E. A.; Csóka, H.; Lazar, I.; Micera, G.; Garribba, E.; Farkas, E. *J. Chem. Soc., Dalton Trans.* **2002**, 2632−2640.

(30) Ni(II): (a) Stemmler, A. J.; Kampf, J. W.; Kirk, M. L.; Pecoraro, V. L. *J. Am. Chem. Soc.* **1995**, *117*, 6368−6369. (b) Arnold, M.; Brown, D. A.; Deeg, O.; Errington, W.; Haase, W.; Herlihy, K.; Kemp, T. J.; Nimir, H.; Werner, R. *Inorg. Chem.* **1998**, *37*, 2920−2925.

(31) Zn(II): Brown, D. A.; Errington, W.; Fitzpatrick, N. J.; Glass, W. K.; Kemp, T. J.; Nimir, H.; Ryan, A. T. *Chem. Commun.* **2002**, 1210−1211.

(32) Co(II): Brown, D. A.; Errington, W.; Glass, W. K.; Haase, W.; Kemp, T. J.; Nimir, H.; Ostrovsky, S. M.; Werner, R. *Inorg. Chem.* **2001**, *40*, 5962−5971.

Table 5. Summary of X-ray Data Collection and Refinement for Hydroxamate Complexes

	8·0.75CH_3CN·0.75Et_2O	**9**	**10·1.5CH_3CN**	**11**
empirical formula	$C_{68.5}H_{69.75}N_{10.75}Cl_2O_{12.75}Mn_2$	$C_{32}H_{30}N_5ClO_6Co$	$C_{35}H_{34.50}N_{6.50}ClO_6Ni$	$C_{32}H_{30}N_5ClO_6Zn$
fw	1428.38	674.99	736.35	681.43
cryst syst	triclinic	monoclinic	monoclinic	monoclinic
space group	$P\bar{1}$	$P2_1/c$	$I2/a$	$P2_1/n$
a (Å)	12.3182(3)	10.9561(4)	14.5773(3)	12.1875(4)
b (Å)	19.6718(3)	18.2711(6)	19.4711(5)	17.0501(3)
c (Å)	28.9826(7)	15.2867(6)	24.8678(5)	14.6762(4)
α (deg)	77.4760(1)			
β (deg)	87.0389(1)	98.5818(18)	103.6499(13)	97.3202(11)
γ (deg)	73.3676(1)			
V (Å^3)	6568.7(2)	3025.83(19)	6859.0(3)	3024.83(14)
Z	4	4	8	4
d_{calcd}, Mg m^{-3}	1.444	1.482	1.426	1.496
temp (K)	150(1)	150(1)	150(1)	150(1)
cryst size (mm^3)	0.23 × 0.20 × 0.10	0.25 × 0.20 × 0.15	0.30 × 0.30 × 0.20	0.35 × 0.28 × 0.08
abs coeff (mm^{-1})	0.539	0.710	0.699	0.954
2θ max (deg)	55.00	54.96	54.92	55.00
reflns collected	39816	11782	13465	12813
indep reflns	28390	6890	7788	6903
variable params	1781	526	564	541
R1/wR2[b]	0.0799/0.1713	0.0413/0.0892	0.0415/0.0922	0.0448/0.1098
GOF (F^2)	1.020	1.057	1.028	1.022
largest diff (e Å^{-3})	1.226/−1.277	0.559/−0.478	0.515/−0.437	0.687/−0.636

[a] Radiation used: Mo Kα (λ = 0.71073 Å). Diffractometer: Nonius KappaCCD. [b] R1 = $\sum||F_o| - |F_c||/\sum|F_o|$; wR2 = $[\sum[w(F_o^2 - F_c^2)^2]/[\sum(F_o^2)^2]]^{1/2}$ where $w = 1/[\sigma^2(F_o^2) + (aP)^2 + bP]$.

hydroxamate in **8A** donates a hydrogen bond to a noncoordinated perchlorate anion (N(5)···O(9) 3.027(7) Å, N(5)−H(5)···O(9) 174.5°).

[(6-Ph_2TPA)Co(ONHC(O)CH_3)]ClO_4 (9). The cobalt hydroxamate complex **9** has a mononuclear structure in the solid state, with all available donors of the 6-Ph_2TPA coordinated to the Co(II) center. A Cambridge Crystallographic Database search (Version 5.24 (Nov 2002)) revealed that only two cobalt hydroxamate complexes, both having bridging hydroxamate ligands, have been previously characterized by X-ray crystallography.[32] In **9**, the Co(II) center has a pseudo-octahedral geometry (Figure 6a), with the hydroxamate coordinated in a hydrophobic sandwich created by the two phenyl substitutents of the 6-Ph_2TPA ligand. The Co−N distances of the phenyl-substituted pyridyl donors are >0.1 Å longer than the Co−N distance of the unsubstituted pyridyl donor. This differentiation in Co−N bond lengths is smaller than that present in the five-coordinate complex **2** (<0.065 Å), and presumably arises in **9** due to increased steric interactions between the phenyl substituents of the two *trans* pyridyl donors (N(3) and N(4)). Two distinct Co−O bond distances are found for **9** (Co(1)−O(1) 2.141(2) Å, Co(1)−O(2) 1.935(2) Å), with the shorter distance being the Co−O interaction *trans* to the tertiary amine nitrogen. The carbonyl-derived oxygen atom (O(1)) of the hydroxamate ligand is positioned *trans* to the unsubstituted pyridyl donor. In this orientation, the hydroxamate N−H moiety lies within the hydrophobic sandwich and forms a hydrogen-bonding interaction (N(5)···O(3) 2.993(3) Å, N(5)−H(5)···O(3) 152(2)°) with the noncoordinated perchlorate anion (Figure S8).

[(6-Ph_2TPA)Ni(ONHC(O)CH_3)]ClO_4·1.5CH_3CN (10·1.5CH_3CN) and [(6-Ph_2TPA)Zn(ONHC(O)CH_3)]ClO_4 (11). Structurally similar mononuclear Ni(II) and Zn(II) hydroxamate complexes (**10·1.5CH_3CN** and **11**) were isolated using the 6-Ph_2TPA ligand. ORTEP representations of the cationic portions of these complexes are shown in Figure 6b,c. Similar to the Co(II) derivative **9**, the divalent metal centers in **10·1.5CH_3CN** and **11** have a distorted octahedral geometry, with the bound hydroxamate positioned between the two phenyl substitutents of the supporting 6-Ph_2TPA chelate ligand. However, the orientation of the hydroxamate binding in **10·1.5CH_3CN** and **11** is reversed with respect to the [(6-Ph_2TPA)M(II)]$^{2+}$ fragment from what is observed for **9**. This leads to the formation of hydrogen-bonded pairs of cations in the solid state for **10·1.5CH_3CN** and **11** (Figure 7), where the two cations are bridged by a six-membered ring involving two hydrogen-bonding interactions. These secondary interactions are each composed of a hydroxamate N−H moiety donating a hydrogen bond to a hydroxamate hydroxyl oxygen bound to the second cation (**10·1.5CH_3CN**, N(5)···O(2) 2.781(2) Å, N(5)−H(5)···O(2) 146(2)°; **11**, N(5)···O(2) 2.746(3) Å, N(5)−H(5)···O(2) 147(3)°).

Complex **10·1.5CH_3CN** is only the second structurally characterized example of a mononuclear nickel hydroxamate complex to be reported, with the previous example having a square pyramidal geometry ([Ni[12]aneN_3-mc2(Ah)]PF_6).[33] In **10·1.5CH_3CN**, the Ni−N_{Py} and Ni−N_{PhPy} bond lengths are very similar to those found for **3·CH_3OH**, indicating that for nickel little change occurs regarding the bonding of the chelate ligand as a consequence of replacement of solvent ligands (CH_3OH and CH_3CN) with an anionic, bidentate chelate ligand. Akin to [Ni[12]aneN_3-mc2(Ah)]PF_6, very similar Ni−O bond lengths are found for the bound hydroxamate anion in **10·1.5CH_3CN** (Ni(1)−O(1) 1.996(1) Å, Ni(1)−O(2) 2.020(2) Å).

(33) Santana, M. D.; García, G.; Pérez, J.; Molins, E.; López, G. *Inorg. Chem*. **2001**, *40*, 5701−5703.

Table 6. Selected Bond Lengths (Å) and Angles (deg) for Hydroxamate Complexes[a]

$[((6\text{-}Ph_2TPA)Mn)_2(\mu\text{-}ONHC(O)CH_3)_2](ClO_4)_2$ (**8·0.75CH$_3$CN·0.75Et$_2$O**)

Cation 8A

Mn(1)−O(1)	2.143(3)	Mn(1)−N(3)	2.277(4)	Mn(2)−O(2)	2.129(3)	Mn(2)−N(8)	2.291(4)
Mn(1)−O(2)	2.269(4)	C(31)−N(5)	1.313(7)	Mn(2)−O(3)	2.144(4)	C(63)−N(10)	1.307(6)
Mn(1)−O(4)	2.142(3)	O(1)−C(31)	1.263(6)	Mn(2)−O(4)	2.252(4)	O(3)−C(63)	1.261(6)
Mn(1)−N(1)	2.308(4)	N(5)−O(2)	1.378(5)	Mn(2)−N(6)	2.297(4)	N(10)−O(4)	1.386(5)
Mn(1)−N(2)	2.394(4)			Mn(2)−N(7)	2.399(4)		
O(1)−Mn(1)−N(2)	146.84(2)	O(4)−Mn(1)−O(2)	77.76(1)	O(3)−Mn(2)−N(7)	152.01(1)	O(4)−Mn(2)−O(2)	78.37(1)
O(1)−Mn(1)−O(2)	73.15(1)	O(4)−Mn(1)−N(2)	82.93(1)	O(3)−Mn(2)−O(4)	73.97(1)	O(2)−Mn(2)−N(7)	83.88(1)
O(1)−Mn(1)−N(1)	83.45(1)	N(3)−Mn(1)−N(2)	72.40(2)	O(3)−Mn(2)−N(6)	83.26(1)	N(8)−Mn(2)−N(7)	71.22(2)
O(1)−Mn(1)−N(3)	135.80(2)	N(3)−Mn(1)−N(1)	100.24(2)	O(3)−Mn(2)−N(8)	128.19(2)	N(8)−Mn(2)−N(6)	102.81(1)
O(1)−Mn(1)−O(4)	96.49(1)	C(31)−O(1)−Mn(1)	115.9(3)	O(3)−Mn(2)−O(2)	100.17(1)	C(63)−O(3)−Mn(2)	115.8(3)
O(2)−Mn(1)−N(1)	145.61(1)	O(1)−C(31)−N(5)	120.9(5)	O(4)−Mn(2)−N(6)	151.60(1)	O(3)−C(63)−N(10)	121.3(5)
N(1)−Mn(1)−N(2)	72.58(1)	O(2)−N(5)−C(31)	118.9(4)	N(6)−Mn(2)−N(7)	71.70(1)	O(4)−N(10)−C(63)	119.4(4)
N(1)−Mn(1)−O(4)	130.74(2)	N(5)−O(2)−Mn(1)	108.5(3)	N(6)−Mn(2)−O(2)	123.07(1)	N(10)−O(4)−Mn(2)	108.4(2)
Mn(1)−O(2)−Mn(2)	101.61(1)	Mn(1)−O(4)−Mn(2)	101.73(1)				

Cation 8B

Mn(3)−O(1A)	2.151(4)	Mn(3)−N(3A)	2.295(4)	Mn(4)−O(2A)	2.137(3)	Mn(4)−N(8A)	2.263(4)
Mn(3)−O(2A)	2.233(3)	C(31A)−N(5A)	1.310(6)	Mn(4)−O(3A)	2.149(3)	C(63A)−N(10A)	1.306(7)
Mn(3)−O(4A)	2.127(3)	O(1A)−C(31A)	1.272(6)	Mn(4)−O(4A)	2.266(3)	O(3A)−C(63A)	1.266(6)
Mn(3)−N(1A)	2.287(4)	N(5A)−O(2A)	1.384(5)	Mn(4)−N(6A)	2.280(4)	N(10A)−O(4A)	1.383(5)
Mn(3)−N(2A)	2.422(4)			Mn(4)−N(7A)	2.394(4)		
O(1A)−Mn(3)−N(2A)	151.26(1)	O(4A)−Mn(3)−O(2A)	79.04(1)	O(3A)−Mn(4)−N(7A)	145.40(1)	O(4A)−Mn(4)−O(2A)	78.09(1)
O(1A)−Mn(3)−O(2A)	73.90(1)	O(4A)−Mn(3)−N(2A)	83.36(1)	O(3A)−Mn(4)−O(4A)	73.31(1)	O(2A)−Mn(4)−N(7A)	81.13(1)
O(1A)−Mn(3)−N(1A)	83.17(1)	N(3A)−Mn(3)−N(2A)	70.79(1)	O(3A)−Mn(4)−N(6A)	83.45(1)	N(8A)−Mn(4)−N(7A)	72.81(2)
O(1A)−Mn(3)−N(3A)	129.45(1)	N(3A)−Mn(3)−N(1A)	103.89(1)	O(3A)−Mn(4)−N(8A)	137.75(1)	N(8A)−Mn(4)−N(6A)	100.32(1)
O(1A)−Mn(3)−O(4A)	99.81(1)	C(31A)−O(1A)−Mn(3)	115.9(3)	O(3A)−Mn(4)−O(2A)	96.28(1)	C(63A)−O(3A)−Mn(4)	116.0(3)
O(2A)−Mn(3)−N(1A)	152.65(1)	O(1A)−C(31A)−N(5A)	120.3(5)	O(4A)−Mn(4)−N(6A)	145.23(1)	O(3A)−C(63A)−N(10A)	120.4(4)
N(1A)−Mn(3)−N(2A)	70.94(1)	O(2A)−N(5A)−C(31A)	119.5(4)	N(6A)−Mn(4)−N(7A)	73.15(1)	O(4A)−N(10A)−C(63A)	119.9(4)
N(1A)−Mn(3)−O(4A)	120.20(1)	N(5A)−O(2A)−Mn(3)	109.2(2)	N(6A)−Mn(4)−O(2A)	130.93(1)	N(10A)−O(4A)−Mn(4)	108.1(3)
Mn(3)−O(2A)−Mn(4)	101.57(1)	Mn(3)−O(4A)−Mn(4)	100.81(1)				

$[(6\text{-}Ph_2TPA)Co(ONHC(O)CH_3)](ClO_4)$ (**9**)

Co(1)−O(1)	2.141(2)	Co(1)−N(4)	2.298(2)	Ni(1)−O(1)	1.996(1)	Ni(1)−N(4)	2.263(2)
Co(1)−O(2)	1.935(2)	O(1)−C(31)	1.268(3)	Ni(1)−O(2)	2.020(2)	O(1)−C(31)	1.272(2)
Co(1)−N(1)	2.103(2)	C(31)−N(5)	1.312(3)	Ni(1)−N(1)	2.056(2)	C(31)−N(5)	1.311(3)
Co(1)−N(2)	2.177(2)	N(5)−O(2)	1.379(2)	Ni(1)−N(2)	2.082(2)	N(5)−O(2)	1.384(2)
Co(1)−N(3)	2.244(2)			Ni(1)−N(3)	2.229(2)		
O(2)−Co(1)−N(2)	175.26(7)	N(4)−Co(1)−O(1)	78.74(6)	O(1)−Ni(1)−N(2)	173.01(6)	N(4)−Ni(1)−O(2)	79.80(6)
O(2)−Co(1)−O(1)	81.17(6)	N(4)−Co(1)−N(2)	78.55(7)	O(1)−Ni(1)−O(2)	82.75(6)	N(4)−Ni(1)−N(2)	81.16(7)
O(2)−Co(1)−N(1)	99.80(7)	N(3)−Co(1)−N(2)	73.66(6)	O(1)−Ni(1)−N(1)	94.67(7)	N(3)−Ni(1)−N(2)	76.37(7)
O(2)−Co(1)−N(3)	102.20(6)	N(3)−Co(1)−N(1)	99.75(7)	O(1)−Ni(1)−N(3)	99.85(6)	N(3)−Ni(1)−N(1)	101.10(7)
O(2)−Co(1)−N(4)	106.17(6)	C(31)−O(1)−Co(1)	107.26(1)	O(1)−Ni(1)−N(4)	104.62(6)	C(31)−O(1)−Ni(1)	110.61(1)
O(1)−Co(1)−N(1)	176.72(6)	O(1)−C(31)−N(5)	120.2(2)	O(2)−Ni(1)−N(1)	176.30(7)	O(1)−C(31)−N(5)	120.43(2)
N(1)−Co(1)−N(2)	78.87(7)	O(2)−N(5)−C(31)	120.71(2)	N(1)−Ni(1)−N(2)	80.45(7)	O(2)−N(5)−C(31)	120.22(2)
N(1)−Co(1)−N(4)	97.98(7)	N(5)−O(2)−Co(1)	109.79(1)	N(1)−Ni(1)−N(4)	98.37(7)	N(5)−O(2)−Ni(1)	105.72(1)

$[(6\text{-}Ph_2TPA)Ni(ONHC(O)CH_3)](ClO_4)$ (**10·1.5CH$_3$CN**)

$[(6\text{-}Ph_2TPA)Zn(ONHC(O)CH_3)](ClO_4)$ (**11**)

Zn(1)−O(1)	2.041(2)	Zn(1)−N(4)	2.219(2)
Zn(1)−O(2)	1.992(2)	O(1)−C(31)	1.269(3)
Zn(1)−N(1)	2.083(2)	C(31)−N(5)	1.304(3)
Zn(1)−N(2)	2.188(2)	N(5)−O(2)	1.382(3)
Zn(1)−N(3)	2.679(2)		
O(1)−Zn(1)−N(2)	169.27(8)	N(4)−Zn(1)−O(2)	89.15(7)
O(1)−Zn(1)−O(2)	82.59(7)	N(4)−Zn(1)−N(2)	76.31(8)
O(1)−Zn(1)−N(1)	90.92(8)	N(3)−Zn(1)−N(2)	72.97(7)
O(1)−Zn(1)−N(3)	103.86(7)	N(3)−Zn(1)−N(1)	91.89(8)
O(1)−Zn(1)−N(4)	110.60(7)	C(31)−O(1)−Zn(1)	109.19(2)
O(2)−Zn(1)−N(1)	164.38(8)	O(1)−C(31)−N(5)	120.80(2)
N(1)−Zn(1)−N(2)	79.05(8)	O(2)−N(5)−C(31)	120.70(2)
N(1)−Zn(1)−N(4)	106.45(8)	N(5)−O(2)−Zn(1)	106.67(1)

[a] Estimated standard deviations indicated in parentheses.

The isolation of **11** adds to the growing list of mononuclear zinc hydroxamate complexes to have been discovered. Previously, Vahrenkamp[34] and Cohen[35] have reported mononuclear zinc hydroxamate species, supported by tris(pyrazolyl)borate chelate ligands, that exhibit a five-coordinate zinc center. In **11**, the zinc ion is six-coordinate and has a psuedo-octahedral geometry. While the Zn−N_{Py} distance (Zn(1)−N(1) 2.083(2) Å) is only slightly longer than the corresponding distance in **4·2CH$_3$CN** (Zn(1)−N(1) 2.053(2) Å), the increase in Zn−N_{PhPy} bond lengths in going from **4·2CH$_3$CN** to **11** is much greater. Specifically, whereas Zn−N_{PhPy} distances of 2.139(2) and 2.075(2) Å are observed for **4·2CH$_3$CN**, in **11** these distances elongate to 2.679(2) and 2.219(2) Å, respectively. The longer of these distances, which

(34) Ruf, M.; Weis, K.; Brasack, I.; Vahrenkamp, H. *Inorg. Chim. Acta* **1996**, *250*, 271−281.

(35) (a) Puerta, D. T.; Cohen, S. M. *Inorg. Chem.* **2002**, *41*, 5075−5082. (b) Puerta, D. T.; Cohen, S. M. *Inorg. Chem.* **2003**, *42*, 3423−3430.

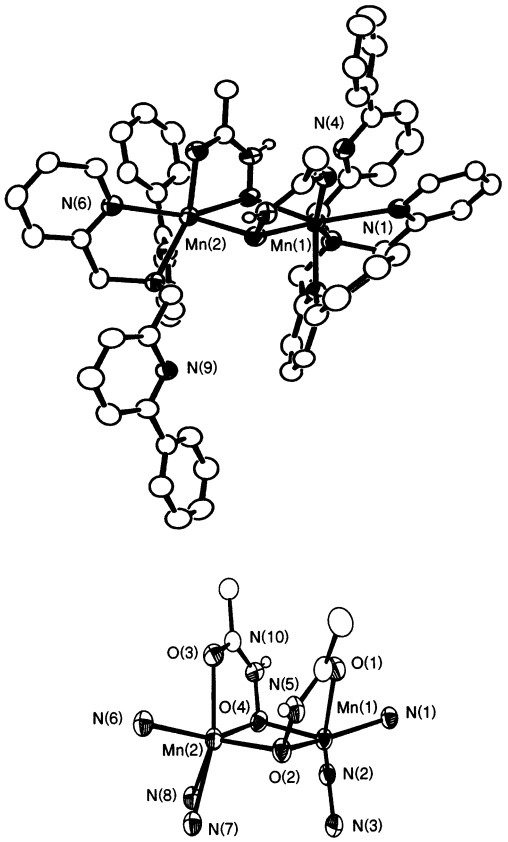

Figure 5. Top: ORTEP representation of one of two dinuclear cations found in the asymmetric unit of **8·0.75CH$_3$CN·0.75Et$_2$O**. All ellipsoids are drawn at the 50% probability level. All hydrogens except the hydroxamate N−H were omitted for clarity. Bottom: ORTEP representation of the dinuclear Mn(II) core.

is for Zn(1)−N(3), suggests only a weak interaction between the zinc center and this phenyl-substituted pyridyl donor. The Zn−O bond lengths in **11** (1.992(2) and 2.041(2) Å) are similar to those reported for monomeric five coordinate zinc hydroxamate complexes (range 1.98−2.10 Å).[34,35]

The methyl group of the bound hydroxamate anion in **10·1.5CH$_3$CN** and **11** is positioned to form CH/π interactions with the phenyl groups of the 6-Ph$_2$TPA ligand (Figures S9 and S10). For both complexes, there is a C(methyl)···arene centroid distance of ∼3.7−3.8 Å (**10·1.5CH$_3$CN**, 3.724 Å; **11**, 3.783 Å), and a second C(methyl)···arene centroid distance that is greater than 4 Å (**10·1.5CH$_3$CN**, 4.13 Å; **11**, 4.46 Å).

Magnetic Moment. The solution magnetic moments of **8**−**10** were measured in CH$_3$CN solution at 298 K using the Evans[11] method (Table 7). For **8**, the μ_{eff} value of 5.6 μ_B/Mn(II) is slightly lower than the spin-only magnetic moment (5.9 μ_B) for an isolated high-spin Mn(II) ion. For **9** and **10**, the observed magnetic moments, μ_{eff} = 4.4 and 3.2 μ_B, respectively, are slightly higher that the spin-only values calculated for high-spin Co^{2+} (3.9 μ_B) and Ni^{2+} (2.8 μ_B) due to spin−orbit coupling.[25]

UV−Vis Spectroscopy. Comparison of the UV−vis spectral features of the solvent-coordinated complex **2** ([(6-Ph$_2$TPA)Co(CH$_3$CN)](ClO$_4$)$_2$) with those of **9** in the region of 500−600 nm (Figure S11) reveals a higher extinction coefficient for the ligand field transition found at ∼570 nm

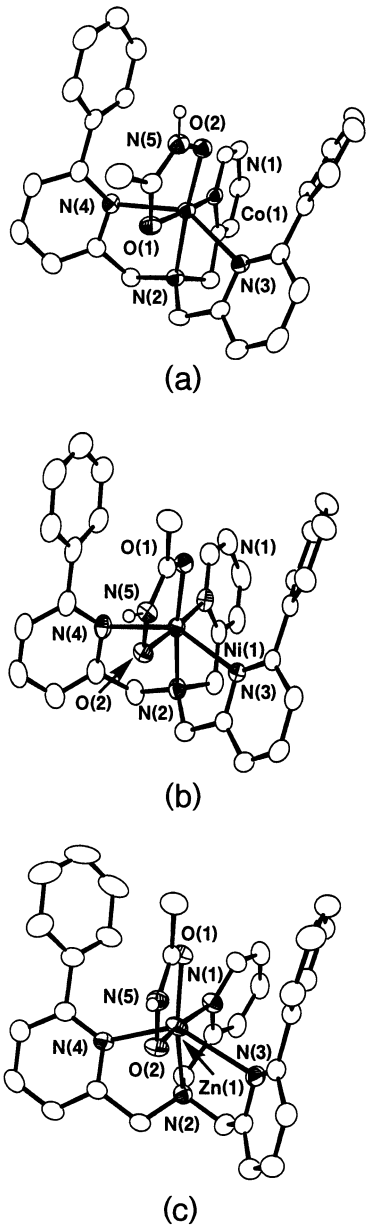

Figure 6. ORTEP representations of the cationic portions of **9**, **10·1.5CH$_3$CN**, and **11**. All ellipsoids are drawn at the 50% probability level. Hydrogen atoms, except the hydroxamate N−H, are not shown for clarity.

(90 M^{-1} cm^{-1}) in **2**, versus the extinction coefficient found for a similar transition in the spectrum of **9** (562 nm (30 M^{-1} cm^{-1}), Table 7). This is consistent with the increase in coordination number for the Co(II) center from five to six upon hydroxamate binding.[36] The octahedral Ni(II) complexes **3** and **10** show differences in the energy of both the $^3A_{2g} \rightarrow {}^3T_{1g}$ and $^3A_{2g} \rightarrow {}^3T_{2g}$ transitions. The latter, found at ∼1007 nm in **3**, is shifted into the near-IR region in **10**. The former transition is also shifted to lower energy upon hydroxamate coordination.

EPR and ^{1}H NMR Spectroscopy. The EPR spectrum of **8** was recorded at 70(1) K (Figure S12). The general features

(36) McMillin, D. R. Electronic Absorption Spectroscopy. In *Physical Methods in Bioinorganic Chemistry: Spectroscopy and Magnetism*; Que, L., Jr., Ed.; University Science Books: Sausalito, CA, 2000; pp 1−58.

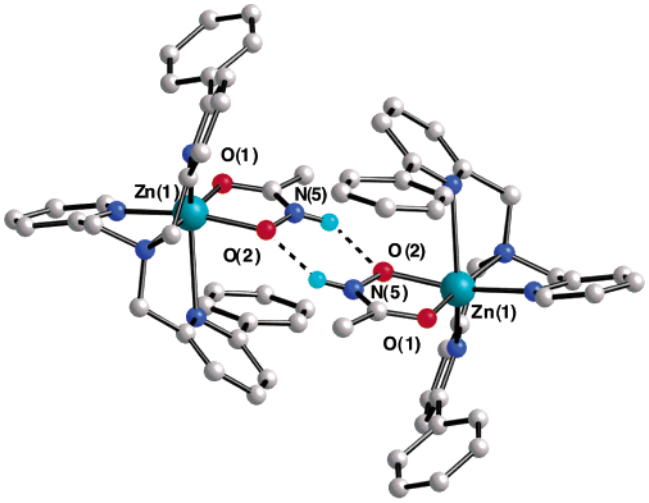

Figure 7. Representation of the hydrogen-bonded cations found in the solid state structure of **11**. Similar hydrogen-bonding interactions are found in **10·1.5CH$_3$CN**.

Table 7. Selected Physical Properties of **8**−**11**

	8	9	10	11
UV−vis, nm (ϵ, M^{-1} cm^{-1})[a]		472 (110) 562 (30) 925(6)	585 (13) 1004 (5)	
μ_{eff}[b] (μ_B)	5.6/Mn(II)	4.4	3.2	
FTIR[c] (cm^{-1})				
$\nu_{C=O}$	1617	1597	1598	1597
ν_{X}[d]	1095 623	1096 623	1097 623	1093 623

[a] Spectra collected in dry CH_3CN. [b] Average value of two independent determinations at 298 K by the Evans method: Evans, D. F. *J. Chem. Soc.* **1959**, *115*, 2003. [c] Spectra collected as dilute KBr pellets. [d] Vibrations of counterion.

of this spectrum are similar to those observed in the solid state spectrum of [(bpmp)Mn$_2$(μ-OAc)$_2$]ClO$_4$ (bpmp = 2,6-bis[bis(2-pyridylmethyl)aminomethyl]-4-methylphenol).[37]

The ^{1}H NMR of **11** in CD_3CN at ambient temperature exhibits a methyl resonance at 1.46 ppm associated with the bound hydroxamate ligand. This resonance is shifted by 0.34 ppm upfield of that observed for free acetohydroxamic acid (1.80 ppm) under identical conditions and is consistent with the presence of CH/π interactions involving this methyl group and the phenyl rings of the 6-Ph$_2$TPA ligand. Further evidence for these secondary interactions was found in the ^{13}C{^{1}H} spectrum of **11**, where the methyl carbon of the acetohydroxamate ligand is found at 17.9 ppm, which is again upfield of the same resonance found for the free acid (19.6 ppm) under identical conditions.

Discussion

Several ligand systems have been reported that provide a hydrophobic coordination environment surrounding one or more open coordination sites on mononuclear metal centers.[38−43] Particularly interesting are recent examples of tetrahedral copper and zinc complexes constructed by Reinaud and co-workers using functionalized calix[6]arene-type ligands. Members of this family of complexes include structural models for substrate-bound species in copper and zinc metalloenzymes, with the calixarene ligand serving as a type of hydrophobic channel to the metal center. Notably, these functionalized calix[6]arene-type ligands, as well as trispyrazolylborate derivatives, generally enforce coordination numbers of four to five, with the latter generally being found for chelate anions.[35] In the work described herein, we have evaluated whether aryl-appended TPA ligands will enable the isolation of mononuclear divalent metal complexes having the following: (1) a hydrophobic environment surrounding a metal center that has one or more solvent-occupied coordination sites, (2) stability with respect to oxidation by dioxygen, and (3) an ability to maintain a mononuclear structure in derivative complexes having a coordinated chelating anion. Such features are key if aryl-appended TPA ligands are to be utilized to produce synthetic models for species relevant to several recently reported metalloenzymes.

Mechanistic pathways proposed for the mononuclear Mn(II) centers in oxalate oxidase and decarboxylase involve interaction of a N$_3$(His)O(Glu)-ligated Mn(II) center with both oxalate and dioxygen through the displacement of two water ligands, leading to the oxidation of Mn(II) to Mn(III).[3a,44] During catalytic turnover, it is suggested that the manganese centers in oxalate oxidase and decarboxylase likely exhibit a coordination number of five or six.[45] As an approach toward generating complexes relevant to oxalate oxidases and decarboxylases, we initiated studies to evaluate the divalent manganese chemistry of aryl-appended TPA ligands. In the Mn(II) derivatives **1** and **8**, the 6-Ph$_2$TPA ligand coordinates only via one of the phenyl-substituted pyridyl donors, leaving three coordination sites available for methanol or anion binding. This coordination mode of the chelate ligand may explain why a dinuclear Mn(II) hydrox-

(37) Blanchard, S.; Blondin, G.; Rivière, E.; Nierlich, M.; Girerd, J.-J. *Inorg. Chem.* **2003**, *42*, 4568−4578.

(38) (a) Blanchard, S.; Le Clainche, L.; Rager, M.-N.; Chansou, B.; Tuchagues, J. P.; Duprat, A. F.; Le Mest, Y.; Reinaud, O. *Angew. Chem., Int. Ed.* **1998**, *37*, 2732−2735. (b) Rondelez, Y.; Sénèque, O.; Rager, M.-N.; Duprat, A. F.; Reinaud, O. *Chem. Eur. J.* **2000**, *6*, 4218−4226. (c) Sénèque, O.; Rager, M.-N.; Giorgi, M.; Reinaud, O. *J. Am. Chem. Soc.* **2000**, *122*, 6183−6189. (d) Le Clainche, L.; Giorgo, M.; Reinaud, O. *Eur. J. Inorg. Chem.* **2000**, 1931−1933. (e) Le Clainche, L.; Giorgi, M.; Reinaud, O. *Inorg. Chem.* **2000**, *39*, 3436−3437. (f) Sénèque, O.; Giorgi, M.; Reinaud, O. *Chem. Commun.* **2001**, 984−985. (g) Sénèque, O.; Rager, M.-N.; Giorgi, M.; Reinaud, O. *J. Am. Chem. Soc.* **2001**, *123*, 8442−8443. (h) Sénèque, O.; Rondelez, Y.; Le Clainche, L.; Inisan, C.; Rager, M.-N.; Giorgi, M.; Reinaud, O. *Eur. J. Inorg. Chem.* **2001**, 2597−2604. (i) Rondelez, Y.; Bertho, G.; Reinaud, O. *Angew. Chem., Int. Ed.* **2002**, *41*, 1044−1046. (j) Sénèque, O.; Campion, M.; Douziech, B.; Giorgi, M.; Rivière, E.; Journaux, Y.; Le Mest, Y.; Reinaud, O. *Eur. J. Inorg. Chem.* **2002**, 2007−2014. (k) Rondelez, Y.; Rager, M.-N.; Duprat, A.; Reinaud, O. *J. Am. Chem. Soc.* **2002**, *124*, 1334−1340.

(39) Kersting, B. *Angew. Chem., Int. Ed.* **2001**, *40*, 3988−3990.

(40) Wieser-Jeunesse, C.; Matt, D.; De Cian, A. *Angew. Chem., Int. Ed.* **1998**, *37*, 2861−2864.

(41) Ooi, T.; Kondo, Y.; Mauroka, K. *Angew. Chem., Int. Ed.* **1998**, *37*, 3039−3041.

(42) Hecht, S.; Fréchet, J. M. J. *Angew. Chem., Int. Ed.* **2001**, *40*, 74−91.

(43) (a) Ruf, M.; Vahrenkamp, H. *Inorg. Chem.* **1996**, *35*, 6571−6578. (b) Kitajima, N.; Tolman, W. B. *Prog. Inorg. Chem.* **1995**, *43*, 419−531. (c) Weis, K.; Vahrenkamp, H. *Eur. J. Inorg. Chem.* **1998**, 271−274.

(44) Reinhardt, L. A.; Svedruzic, D.; Chang, C. H.; Cleland, W. W.; Richards, N. G. J. *J. Am. Chem. Soc.* **2003**, *125*, 1244−1252.

(45) Whittaker, M. M.; Whittaker, J. W. *JBIC, J. Biol. Inorg. Chem.* **2002**, *7*, 136−145.

amate complex having μ-η^1:η^2-ONHC(O)CH_3 coordination is isolated, versus mononuclear hydroxamate derivatives for the other 3d metal ions (Co(II), Ni(II), and Zn(II)), where all available donors of the 6-Ph_2TPA ligand interact with the divalent metal center. Tridentate coordination of the 6-Ph_2TPA ligand does not impart a significant degree of hydrophobic character or steric hindrance around the manganese centers in **1** and **8**, and this differs from that found for 6-Me_3TPA in synthetic Mn(II) complexes having a bound monoanionic or dianionic catecholate ligand, wherein tetradentate N_4 coordination is observed.[18g] Determination of the nuclearity of **8** in solution, as well as further EPR studies of this complex, is currently in progress.[39,46]

The coordination chemistry of the aryl-appended TPA ligands with Ni(II), Co(II), and Zn(II) differs dramatically from that observed for Mn(II). In all of the complexes isolated of these metals, each of the donor atoms available on the aryl-appended TPA chelate ligand coordinates to the metal center to produce mononuclear structures. For the solvent adducts **2**−**6**, while divalent cobalt and zinc complexes (**2**, **4**, and **6**) each have a coordination number equal to five, with only one bound solvent molecule, the divalent nickel complexes **3** and **5** have six-coordinate structures. For **2**, **4**, and **6**, the aryl appendages of the 6-Ph_2TPA and 6-$(Me_2Ph)_2$TPA ligands form CH/π interactions with the methyl group of the bound acetontrile ligand. These interactions are detectable by ^{1}H NMR spectroscopy when zinc complexes **4** and **6** are dissolved in CD_3NO_2 solution, as an upfield shifted acetonitrile methyl resonance, consistent with the presence of CH/π interactions, is present in spectra of both complexes. It is important to note that a similar resonance is not found in ^{1}H NMR spectra of [(TPA)Zn(CH_3CN)]-$(ClO_4)_2$ (**7**) collected under identical conditions. This indicates a unique hydrophobic influence on the solvent-occupied coordination site by the aryl substituents in the 6-Ph_2TPA and 6-$(Me_2Ph)_2$TPA ligands found in **2**, **3**, and **5**. Notably, the six coordinate Ni(II) center in **4** exhibits a sandwich type motif, wherein a bound acetonitrile molecule is positioned between the aryl substitutents of the 6-Ph_2TPA ligand. This results in the formation of two shorter CH/π interactions (C(33)$\cdots$arene centroid distances of 3.66 and 3.63 Å) than are found in the Co(II) and Zn(II) analogues.

Examination of the electrochemical properties of the cobalt and nickel complexes **2**, **3**, and **5** revealed reversible couples corresponding to the reduction of the +2 metal complexes, presumably to +1. No oxidative couples were found for M(II)/M(III) in this family of complexes. The electrochemical properties of these complexes are consistent with studies reported by Canary and co-workers of copper derivatives of phenyl-appended tris((pyridyl)methyl)amine ligands.[6b] In a study of the redox properties of four copper(II) complexes that differed in the number of phenyl-appended pyridyl donors present from zero to three ([(TPA)Cu(CH_3CN)]-$(ClO_4)_2$, [(6-PhTPA)Cu(CH_3CN)]$(ClO_4)_2$, [(6-Ph_2TPA)Cu-(CH_3CN)]$(ClO_4)_2$, and [(6-Ph_3TPA)Cu(CH_3CN)]$(ClO_4)_2$), the Cu(II)/Cu(I) redox potential in CH_3CN solution was found to increase by ~100 mV for each phenyl substituent present. This behavior was attributed primarily to the fact that the phenyl appendages reduce the local dielectric by shielding the metal center from the polar solvent, thus favoring a lower oxidation state for the metal. Other factors considered by Canary and co-workers included the effect of steric interactions involving the phenyl substituents, and the difference in σ-donor properties between pyridyl and phenyl-appended pyridyl donors. However, comparison of the X-ray crystallographically characterized Cu(II) and Cu(I) complexes [(6-Ph_3TPA)Cu(CH_3CN)]$(ClO_4)_2$ and [(6-Ph_3TPA)Cu]BPh_4 revealed only minor structural perturbations resulting from reduction of the metal center, inconsistent with the increase in redox potential for [(6-Ph_3TPA)Cu(CH_3CN)]$(ClO_4)_2$ (300 mV vs NHE) versus [(TPA)Cu(CH_3CN)]$(ClO_4)_2$ (0.00 mV vs NHE). In addition, literature precedent suggests that the introduction of a phenyl substituent to a pyridyl donor should impart only a small inductive effect.[47] It was on the basis of these combined analyses that Canary et al. concluded that environmental effects were the primary reason for the more positive reduction potentials observed for phenyl-appended tris((pyridyl)methyl)amine copper complexes. In regard to the metal complexes reported herein, investigation of additional derivatives (e.g., TPA and 6-PhTPA analogues) is necessary to fully evaluate the influence of phenyl substituents on the redox properties of tris((pyridyl)methyl)amine-ligated Mn(II), Co(II), and Ni(II) complexes.[48] Finally, the electrochemical properties of the nickel derivatives **3** and **5** are consistent with the observation that nitrogen/oxygen-ligated Ni(II) centers typically do not undergo oxidation in a biologically relevant redox range. Notably, X-ray absorption spectroscopic studies of the nickel-containing acireductone dioxygenase (ARD), wherein the active site metal center is ligated by a mixture of nitrogen and oxygen donors, do not indicate any change in redox level upon substrate binding, thus suggesting a non-redox role for the metal center in this enzyme.[4b]

Admixture of the 6-Ph_2TPA ligand, $M(ClO_4)_2 \cdot 6H_2O$, and $Me_4NOH \cdot 5H_2O$ in methanol solution, followed by the addition of an equimolar amount of acetohydroxamic acid, yielded the mononuclear hydroxamate complexes [(6-Ph_2-TPA)Co(ONHC(O)CH_3)]$(ClO_4)_2$ (**9**), [(6-Ph_2TPA)Ni(ONHC-(O)CH_3)]$(ClO_4)_2$ (**10**), and [(6-Ph_2TPA)Zn(ONHC(O)CH_3)]-$(ClO_4)_2$ (**11**), all of which were characterized by X-ray crystallography. Isolation of these hydroxamate complexes indicates that use of the 6-Ph_2TPA ligand system enables

(46) The magnetic and EPR properties of dinuclear Mn(II) complexes are of interest toward understanding features of the dinuclear manganese sites found in several enzymes including arginase and catalase: (a) Dubois, L.; Xiang, D.-F.; Tan, X.-S.; Pécaut, J.; Jones, P.; Baudron, S.; Le Pape, L.; Latour, J.-M.; Baffert, C.; Chardon-Noblat, S.; Collomb, M.-N.; Deronzier, A. *Inorg. Chem.* **2003**, *42*, 750−760 and references therein. (b) Howard, T.; Telser, J.; DeRose, V. J. *Inorg. Chem.* **2000**, *39*, 3379−3385. (c) Hureau, C.; Anxolabehere-Mallart, E.; Nierlich, M.; Gonnet, F.; Riviere, E.; Blondin, G. *Eur. J. Inorg. Chem.* **2002**, *10*, 2710−2719.

(47) (a) James, B. R.; Williams, R. J. P. *J. Chem. Soc.* **1961**, 2007−2019. (b) Sorrell, T. N.; Jameson, D. L. *Inorg. Chem.* **1982**, *21*, 1014−1019.

(48) Solvent-coordinated tris((pyridyl)methyl)amine complexes of Ni(II) and Co(II) akin to **2**, **3**, and **5** have been structurally characterized; however, the electrochemical properties of these complexes were not reported.[20c,23c]

the generation of novel mononuclear divalent metal complexes of nickel, zinc, and cobalt having a single chelating anion. These structures are reminiscent of proposed substrate adducts in Ni^{2+}-containing ARD and Zn^{2+}- and Ni^{2+}-containing glyoxalase I. Thus, further studies of nickel and zinc complexes of these aryl-appended TPA ligands with acidreductone and hemithioacetal model substrates are clearly warranted.

Concluding Remarks

The 6-Ph_2TPA and 6-$(Me_2Ph)_2$TPA ligands employed in this study are easily prepared in multigram quantities via straightforward synthetic procedures. As shown by the isolation of novel hydroxamate derivatives, these ligands enable the isolation of interesting mononuclear complexes with hydrophobic encapsulation of a metal-bound chelating anion.

Acknowledgment. We acknowledge the support of the Herman Frasch Foundation (501-HF02 to L.M.B.) and the National Science Foundation (CAREER Award CHE-0094066 to L.M.B.; CHE-0078746 to J.A.H.).

Supporting Information Available: ORTEP representations showing CH/π interactions in **1A·CH_3OH**, **1B·$2CH_3OH$**, **2·$2CH_3CN$**, **3·CH_3OH**, **4·$2CH_3CN$**, **10·$1.5CH_3CN$**, and **11**; Chem3D space-filling figure of **9**; EPR spectra for **1** and **8**; cyclic voltammograms for **2**, **3**, and **5**; X-ray crystallographic files (CIF) for complexes **1A·CH_3OH**, **1B·$2CH_3OH$**, **2·$2CH_3CN$**, **3·CH_3OH**, **4·$2CH_3CN$**, **6·$2.5CH_3CN$**, **7·CH_3CN**, **8·$0.75CH_3CN$·$0.75Et_2O$**, **9**, **10·$1.5CH_3CN$**, and **11**. This material is available free of charge via the Internet at http://pubs.acs.org.

IC034810Y